Research Square

Preprints are preliminary reports that have not undergone peer review.
They should not be considered conclusive, used to inform clinical practice,
or referenced by the media as validated information.

Experimental Investigation on Performance, Emission, and Tribological Characteristics of Waste Plastic Oil Blends With Various Metal Oxide Nanoparticles in a Diesel Engine

Thirugnanasambantham Rajamanickam
Department of Mechanical Engineering, Dhanalakshmi Srinivasan Engineering College (Autonomous), Perambalur 621212, Tamil Nadu

Santhoshkumar Annamalai
Department of Mechanical Engineering, SRM Institute of Science and Technology, Ramapuram, Chennai 600089, Tamil Nadu,

Jayakumar Thangamani
Department of Mechanical Engineering, Dhanalakshmi Srinivasan Engineering College (Autonomous), Perambalur 621212, Tamil Nadu

Arunprasad Jayaraman
arunprasad.jayaraman@wits.ac.za

School of Mechanical, Industrial & Aeronautical Engineering, University of the Witwatersrand, Johannesburg https://orcid.org/0000-0002-5220-1344

Research Article

Keywords: Waste plastic oil, Pyrolysis, Metal oxides, Performance, Emission, Tribology

Posted Date: July 23rd, 2026

DOI: https://doi.org/10.21203/rs.3.rs-10165838/v1

License: This work is licensed under a Creative Commons Attribution 4.0 International License.
Read Full License

Experimental Investigation on Performance, Emission, and Tribological Characteristics of Waste Plastic Oil Blends With Various Metal Oxide Nanoparticles in a Diesel Engine

Thirugnanasambantham Rajamanickam [1], Santhoshkumar Annamalai[2], Jayakumar Thangamani[1], Arunprasad Jayaraman[3,4]*

[1]Department of Mechanical Engineering, Dhanalakshmi Srinivasan Engineering College (Autonomous), Perambalur 621212, Tamil Nadu, India.

[2]Department of Mechanical Engineering, SRM Institute of Science and Technology, Ramapuram, Chennai 600089, Tamil Nadu, India.

[3]School of Mechanical, Industrial and Aeronautical Engineering, University of the Witwatersrand, Johannesburg 2000, South Africa.

[4]Centre for Research and Innovation, Academy of Maritime Education and Training (AMET) Deemed to be University, Kanathur, Chennai 603112, Tamil Nadu, India.

*Corresponding author email: **arunprasad.jayaraman@wits.ac.za**

Abstract

This study investigates the effect of various nanoparticles on the performance and emission characteristics of a diesel engine fueled with waste plastic oil (WPO) blends. Five fuel samples were prepared and tested: diesel, WPO20, WPO20+50 ppm MgO, WPO20+50 ppm RuO_2, and WPO20+50 ppm La_2O_3. Experiments were conducted on a single-cylinder, four-stroke, water-cooled, direct-injection diesel engine coupled to an eddy-current dynamometer under controlled-load conditions. The nanoparticles were characterized using TEM analysis, confirming their morphology. At peak load, the WPO20+50 ppm MgO blend exhibited a 3.53% increase in BTE and a 15.5% reduction in BSFC compared to WPO20, indicating improved combustion efficiency. Emission results showed significant reductions of 20.97% in CO, 27.96% in HC, and 13.76% in smoke opacity, while NO_X emissions increased slightly by 7.07% due to higher in-cylinder combustion temperatures and enhanced oxidation activity. Tribological performance was evaluated using a four-ball tribometer under a 40 kg load, 1200 rpm, and 75 °C for 3600 s. The WPO20+50 ppm MgO blend showed a 12.1% reduction in COF and a 22.9% reduction in WSD, indicating improved lubricity and anti-wear performance. SEM analysis of worn surfaces revealed smoother tracks with fewer grooves and reduced surface deformation in nanoparticle-doped fuels, confirming the formation of a protective tribo-film. Overall, the results demonstrate that the addition of MgO nanoparticles significantly enhances engine performance, reduces emissions, and improves tribological behaviour, making WPO-based blends a promising sustainable fuel for diesel engines.

Keywords: Waste plastic oil, Pyrolysis, Metal oxides, Performance, Emission, Tribology.

Nomenclature

Al_2O_3	- Aluminium oxide
ASTM	- American society for testing and materials
AWSD	- Average wear scar diameter
BTE	- Brake thermal efficiency
BSFC	- Brake-specific fuel consumption
CeO_2	- Cerium oxide
CO	- Carbon monoxide
COF	- Coefficient of friction
CuO	- Copper oxide
GNP	- Graphene nanoplatelets
GQD	- Graphene quantum dots
GT	- Gigaton
h-BN	- Hexagonal boron nitride
HC	- Hydrocarbons
HRR	- Heat release rate
kg	- Kilogram
kW	- Kilowatt
La_2O_3	- Lanthanum oxide
MgO	- Magnesium oxide
MT	- Metric ton
NO_X	- Nitrogen oxides

PPO - Plastic pyrolysis oil
PO - Plastic oil
ppm - Parts per million
rpm - Revolutions per minute
SEM - Scanning electron microscopy
TiO_2 - Titanium dioxide
ULDP - Used low-density polyethylene oil
WCPO - Waste cable pyrolysis oil
WPO - Waste plastic oil
WS_2 - Tungsten disulfide
WTPO - Waste tire pyrolysis oil
WPO20 - Blend of 80% diesel+20% WPO
WPO20+50 ppm MgO - WPO20+50 ppm magnesium oxide
WPO20+50 ppm RuO_2 - WPO20+50 ppm ruthenium oxide
WPO20+50 ppm La_2O_3 - WPO20+50 ppm lanthanum oxide
ZnO - Zinc oxide

1. Introduction

The widespread applications of plastics in industry, household items, and engineering components are largely due to their high versatility and mechanical strength. The most used polymers are polyethylene, polypropylene, polystyrene, polyvinyl chloride, polyurethane, and polyethylene terephthalate (Wechselberger et al. 2026). Waste plastic accumulation has been increasing worldwide, from about 275 MT in 2012 to nearly 460 MT in 2019, and will continue to rise to nearly 1231 MT by 2060 if this trend persists (Drobne et al. 2026). Significant amounts of related to discarded plastics end up at waste disposal sites and are released into the natural surroundings, causing plastic pollution in both terrestrial and aquatic environments (Anand et al. 2026). Plastics do not readily biodegrade and ultimately become microplastics and nanoplastics in environmental compartments. These pollutants bioaccumulate in trophic chains and affect aquatic ecosystems, thereby reducing biodiversity (Afroze et al. 2026). Furthermore, the long-term presence of plastic-related toxic chemicals within the ground and contamination of groundwater may create serious concerns for ecosystems and public well-being. Meanwhile, the same time, the world's energy demand continues to grow as developing countries industrialize, urbanize and experience population growth. Transportation is a key driver of economic growth, and it remains highly dependent on petroleum-based liquid fuels, largely due to the fuels' high energy density and the existing infrastructure (Yadav et al. 2025). However, fossil fuels are finite, unequally distributed, and subject to volatile prices, making it questionable whether this energy system can be sustained in the long term. Diesel engines find broad application in transportation systems, agriculture, as well as manufacturing industries because of theirlongevity, reliability, and heat conversion efficiency.Conversely, diesel combustion pollutes the environment as it contributes to air quality degradation, global warming, and diseases (Wierzbicki et al. 2026). Thus, alternative fuels from sustainable sources need to be developed. Waste-derived fuels such as waste fuel derived from plastic waste, which can be described as produced through the process generated through the pyrolytic conversion of non-biodegradable plastic waste in an oxygen-depleted, thermochemical environment, have attracted global attention as it provides an approach to both discarded plasticsdisposal and energy generation (Ahmad et al. 2024; Januszewicz et al. 2023). It is also suitable for CI engines with a few modifications. WPO has several technical disadvantages including high viscosity, low volatility, and poor atomization, resulting ininadequate blending of air and fuel along with incomplete burning process (Yim et al. 2025; Saha et al. 2021). As a result, WPO based fuels are also associated with higher emissions of HC, CO, and PM also reduce the BTE, compared to conventional diesel; and their poor lubricity characteristics contribute to higher mechanical losses and wear of engine’s components, which can indirectly affect engine mechanical efficiency and lifetime (Paul et al. 2026). However, there are some restrictions to overcome, because in recent years, Numerous studies have investigated the application of nanoparticles as fuel additives (Gnanamoorthi et al. 2022). The high surface area, high heat transfer capability, and strong catalytic performance of the nanoparticles, when combined, enhance the fuel's reactivity. They improve atomization, enhance oxidation reactions, shorten ignition lag, and increase burning efficiency. As a result, considerable enhancements in engine performance along with reductions in

harmful emissions are widespread (Livingston et al. 2025). The results, however, vary across studies, indicating a lack of uniformity and the need for a systematic understanding (Polat et al. 2022). Table 1 Summary of earlier studies regarding performance evaluation and emission behaviour of nanoparticles used in the WPO. According to prior research, nanoparticles enhance the combustion performance of WPO and considerably reduce exhaust emissions.

In addition to combustion properties, the tribological properties of fuels are also important the operational efficiency of an engine. Mechanical resistance and wear directly affect the fuel efficiency and durability of the power unit. Engine tribology is the study of the lubricating films formed by the fuels on the surfaces of the piston rings, cylinder liners and bearings. Poor lubrication may result in adhesive wear, abrasive wear, surface fatigue and increased frictional losses (Lyu et al. 2026). Pyrolytic oil from Waste plastic fuel possesses lower lubricating ability than conventional diesel because pyrolysis distorts the structure of hydrocarbons in the oil, resulting in less favorable boundary lubrication conditions (Yaqoob et al. 2022; Baskar et al. 2019). To solve this problem, nanoparticles have been developed as multifunctional additives to improve both combustion and tribological properties (Verma et al. 2008). Nanoparticles can form a protective tribofilm at the rubbing surfaces, reduce direct contact between metallic surfaces, increase applied force carrying capability and reduce friciton. material deterioration surface damage is less severe under similar sliding conditions to an engine (Peña-Parás et al. 2015). Table 2 Summary of previous study of tribology behaviour of nanoparticles used in the WPO blends.

In the past, several metal oxide nanoparticles have been shown to enhance the tribological properties of blends of WPO. Investigations related to WPO formulations based on hybrid nanoparticle systems of MgO, RuO_2, and La_2O_3 are still limited in the literature. Moreover, the synergistic effect of these nanoparticles on their performance, emission, and tribological properties has not been systematically explored. Most of the previous studies were conducted independently on either engine performance or tribological characteristics. The study presents a novel approach in which the same fuel formulations are evaluated in a CI power unit for operational performance, exhaust emission properties, and in a four-ball tribometer for tribological behavior. This unified experimental strategy ensures consistency in fuel evaluation and enables a meaningful comparison between engine operating behavior and lubricity-related wear characteristics under laboratory conditions. The present study examines the knowledge gap through investigating the effect of incorporating MgO, RuO_2, and La_2O_3 nanoparticles into WPO20 blends at a fixed dosage of 50 ppm each. The experiments are conducted in both a CI engine and a four-ball tribometer to assess the performance of the engine, emissions, and tribological behavior. The research further seeks to identify the optimal nanoparticle-assisted WPO blend.

Table 1 Existing studies on the influence of nanoparticle additives on the performance and emission behavior of WPO-fueled in CI engine

Fuel samples containing different levels of nanoparticles	Reference Fuel	Out Performed Samples	Performance	Emissions	References
Surgical glove waste pyrolysis oil (SGWPO) with Pentanol, SiO_2 and nanographene 1. Diesel 2. SGWPO 3. SGWPO75P25 4. SGWPO75P25+NSDO 5. SGWPO75P25+NG	SGWPO	SGWPO75P25+ NSDO	BSFC 13.38% ↓ & BTE 9.72% ↑	Emission analysis revealed a 33.06% decrease in CO, a 25.67% reduction in HC, a 29.1% drop in smoke levels, and a 36.81% decrease in NO_x.	(Sathish et al. 2025)
E-waste plastic oil & SiO_2 1. Diesel 2. WPO20 3. WPO20 + SiO_2 40 4. WPO20 + SiO_2 80 5. WPO20 + SiO_2 120	WPO20	WPO20 + SiO_2 120	BSFC 6.9% ↓ & BTE 4.3% ↑	The emissions showed notable improvements, with CO reduced by 18%, HC by 14%, and smoke by 19%. However, NO_x emissions increased slightly by 5.7%.	(Deepankumar et al. 2025)
Waste Plastic Oil & Al_2O_3	WPO10 &	WPO10 +30Al_2O_3	WPO10+ 30Al_2O_3	WPO30+30Al_2O_3 The emissions were reduced,	

1. Diesel 2. WPO10 3. WPO20 4. WPO30 5. WPO10+30Al_2O_3 6. WPO20+30Al_2O_3 7. WPO30+30Al_2O_3	WPO30	& WPO30 +30Al_2O_3	BSFC 13.6% & BTE 2.62%	CO by 37.45%, HC by 22.5 ppm, and smoke by 33.23%. But NO_x emissions increased.	(Thiruselvam et al. 2025)
Used Polymer Pyrolysis oil & Graphite 1. D100 2. UPO20 3. UPO40 4. UPO100 5. UPO20n50 6. UPO20n100	D100	UPO20n100	BSFC 11.6 % & BTE 2.79%	The emissions decreased, with CO reduced by 9.9%, HC by 8.9%, and smoke by 8.9%.	(Sambandam et al. 2024)
Waste Cable Pyrolytic Oil & Graphene 1. Diesel 2. WCPO 3. B20D80G20 4. B20D80G40	NA	A load of 1420 W @ B20D80G40	BSFC 343.79 g/ kWh & BTE 23.17%	The following emission parameters were observed at a load of 1420 kW: CO – 0.048%, HC – 28.74 ppm, NO_x – 455.43 ppm, and CO_2 – 5.13%.	(Canan et al. 2024)
Waste Plastics biodiesel with 1-butanol and CeO_2 1. D100 2. 90D7WPO3B+25 ppm CeO_2 2. 85D10WPO5B+50 ppm CeO_2 3. 80D13WPO7B+75 ppm CeO_2 4. 100WPO+100 ppm CeO_2	D100	NA	90D7WPO3B+25 ppm CeO_2 BSFC 13.66% & BTE 12.25%	80D13WPO7B+75 ppm CeO_2 CO-27.7% 80D13WPO7B+75 ppm CeO_2 CO_2-18.03% 100WPO+100 ppm CeO_2 HC-40%	(Kumar et al. 2024)
Distilled waste plastic oil & Nanographene 1. Diesel 2. 80D2ODPO 3. 80D20DPO50G 4. 80D20DPO70G 5. 80D20DPO100G	80D2ODPO	80D20DPO100G	BSFC 0.331 kg/kWh	NA	(Das et al. 2024)

Table 2 Existing research on the role of metal oxide nanomaterials on the friction-related characteristics of waste-to-fuel

Experimental Samples with Nanoparticles	Base fuel	Tribological Apparatus	Results findings	References
1.PO + GNP (0.5%, 1%, 1.5%, 2%) 2.PO + hBN (0.5%, 1%, 1.5%)	PO	A ball on disk	• The addition of 1.5% GNP to PO resulted in a 54% reduction in the COF and an 85% decrease in WSD. • The worn surfaces were further characterized through Raman spectroscopy to examine their structural changes.	(Sikdar et al. 2023)
1.FTPO + MgO (0.1%, 0.2%) 2.FTPO + Graphene (0.1%, 0.2%) 3. FTPO + Al_2O_3 (0.1%, 0.2%)	FTPO 10	Four-ball tribometer	• The incorporation of 0.1% Al_2O_3 in FTPO10 decreased COF and WSD by 2.83% and 22.09%, respectively. With 0.2% MgO, surface roughness was reduced by 36.2%. • SEM and EDX analyses were conducted to examine the worn surfaces.	(Loo et al. 2023)
1.PO + CuO (0.5%, 1%, 1.5%)+ Mineral oil	PO	A ball on a disk	• PO with 1% CuO reduced the COF by 20%. • PO with 0.5% CuO reduced the WSD by 44%. • Worn surfaces were examined using SEM coupled with EDX analysis.	(Sikdar et al. 2025)

2. ExperimentalMaterials and Procedures

2.1 Pyrolysis process



Fig.1 photograph of the pyrolysis plant

The laboratory-scale pyrolysis equipment used in this study is provided in Fig.1. It consists of a batch-type fixed-bed reactor, a condensation system that is cooled with water, and a vacuum-assisted vapor transport and product collection system. Pyrolysis is a thermochemical process that involves the generation of solid char residues, non-condensable gases, and liquid oil from organic matter (Burra et al. 2024). The WPO production was performed in this study using waste plastics containing a high amount of polyethylene terephthalate and a low amount of polypropylene and high-density polyethylene. The feedstock material was cleaned, dried, and pre-processed into small pieces (0.5-2 inches) to facilitate heat transfer and to minimize thermal stresses. The reactor was made of mild steel, was 63 cm high and 21 cm across, and was designed to resist heat and corrosion. It could be used up to 600 °C in an oxygen-free atmosphere. The electrical heating coils, glass wool insulation, K-type thermocouples, digital temperature controller, and pressure gauge were installed to ensure the system is operating correctly. It was also run at reduced pressures with the aid of a vacuum pump to remove the vapour, allowing the process to be carried out more efficiently. Vapors produced were condensed using a water-cooled stainless-steel condenser with a continuous circulation of water in the condenser, and the condensed liquid fuel is stored in the storage tank. All non-condensing vapors were vented safely and recovered for auxiliary energy generation. The reactor was heated to the reaction temperature range of 500-550 °C, and the retention time of the reaction was 30-60 minutes under an oxygen-free atmosphere. The temperature was then slowly increased and controlled by a digital controller to maintain the temperature within ±10 °C to advantageously thermally crack the feedstock uniformly. About 760 g of a liquid product per kg of the feedstock waste, plastic, and solid char, and a small quantity of non-condensible gases.

2.2 Nanoparticles

The additives used in the present study have different physicochemical and catalytic properties, which result in different combustion behavior, such as MgO, RuO_2, and La_2O_3 nanoparticles. As an oxygen buffering agent, the oxidation kinetics of the MgO nanoparticles are improved, and the local availability of oxygen is increased, thus improving the combustion efficiency. The excellent catalytic activity, high thermal stability, and oxygen mobility of RuO_2 nanoparticles are well known to be beneficial for producing more complete oxidation of the fuel and less incomplete combustion product formation. Apart from this, La_2O_3 is also a rare earth metal oxide that shows high redox activity and radical scavenging potential, which enables interaction with the ROS generated during the combustion of the biodiesel, thereby reducing the emissions and stabilizing the combustion process. These synergic effects of these nanoparticles fuel stability and reduce engine-out emissions of biodiesel blends (Karthikeyan et al. 2018). The physicochemical properties of the nanoparticles are summarized in Table 3.

Table 3 provides an overview of nanoparticle properties.

Parameter	Value/Observation

Supplier	Sigma-Aldrich, Bangalore, India		
Chemical formula	MgO	RuO_2	La_2O_3
Molecular weight (g/mol)	40.3	133.07	325.81
Density (g/cm^3)	3.58	6.97	6.51
Boiling point (°C)	3600	3900	4500
Particle size (nm)	<100	<100	<100
Morphology	Nanorods	Irregular	Spherical

2.3 Preparation of fuel blends

Fig.2 illustrates the fuel preparation process schematically. In the present study, five fuel samples, including pure diesel, were prepared for investigation. Initially, a base blend (WPO20) was prepared by combining 80% diesel and 20% WPO by volume, with magnetic stirring to ensure uniform dispersion. Subsequently, the WPO20 blend was modified by incorporating MgO, RuO_2 and La_2O_3 nanoparticles present at a concentration of 50 ppm each. The resulting mixtures were then subjected to ultrasonication at 40 kHz and 500 W for 30 minutes to achieve stable and homogeneous nanoparticle dispersion within the fuel matrix. Table 4 summarizes the volumetric composition of diesel, WPO, and different nanoparticles, while an overview of the physicochemical properties of the formulated fuel blends are presented in Table 5.

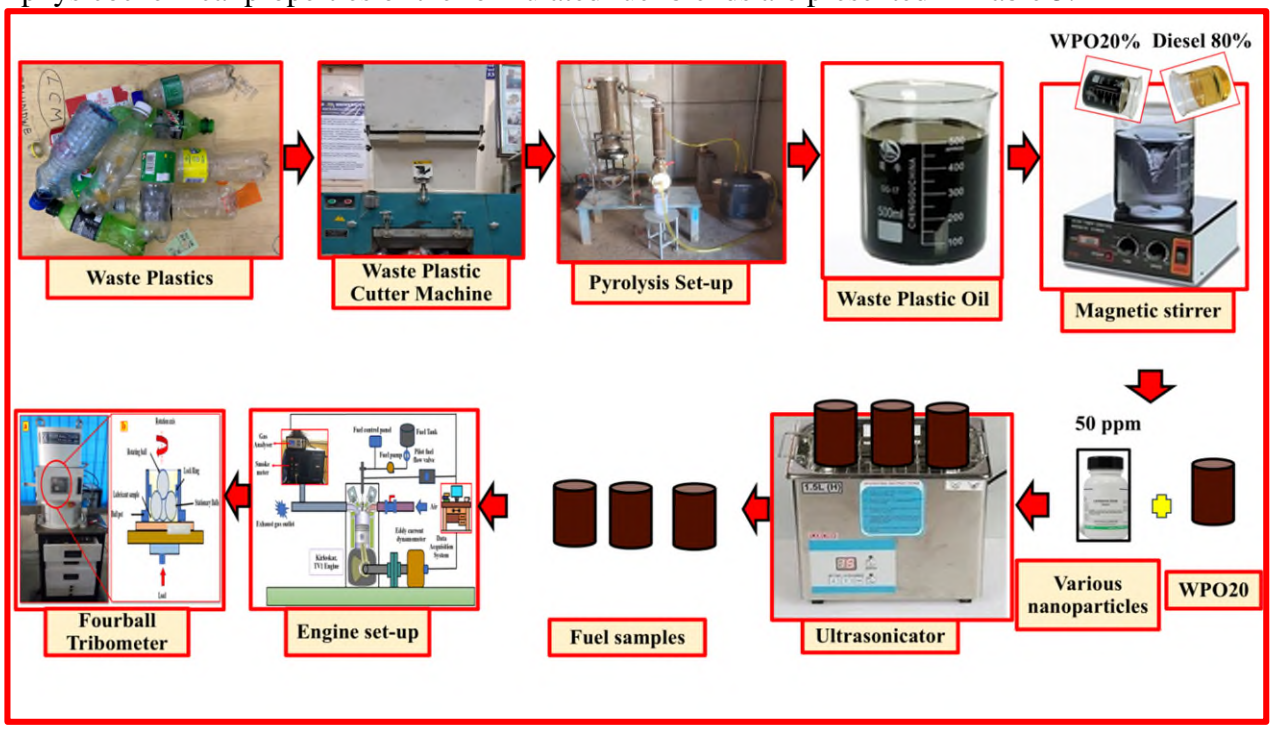


Fig.2 illustrates the complete fuel preparation process, including the experimental setup.

Table 4 illustrates the volumetric proportions of diesel and WPO used to prepare fuel blends.

Fuel Samples	WPO (% by volume)	Diesel (% by volume)	MgO nanoparticle (ppm)	RuO_2 nanoparticle (ppm)	La_2O_3 nanoparticle (ppm)
Diesel	-	100	-	-	-
WPO20	20	80	-	-	-
WPO20+50 ppm MgO	20	80	50	-	-
WPO20+50 ppm RuO_2	20	80	-	50	-
WPO20+50 ppm La_2O_3	20	80	-	-	50

Table 5 shows the physicochemical properties of the prepared fuel blends.

Property	Density measured at 15°C (kg/m^3)	Kinematic viscosity determined at 40°C	Calorific value (kJ/kg)	Flash point temperature (°C)	Cetane number of the fuel
Diesel	835	2.54	43150	49	45

WPO20	828	2.72	42171	54	44.2
WPO20+50 ppm MgO	841	2.91	42869	66	47
WPO20+50 ppm RuO_2	835	2.85	42744	62	46
WPO20+50 ppm La_2O_3	832	2.81	42582	60	45

2.4 Experimental details

The test engine was a single-cylinder, water-cooled, direct-injection, four-stroke diesel engine having a compression ratio of 17.5:1. The power unit produced a power output corresponding to 5.2 kW and had a bore of 80 mm and a cycle of 120 mm. The power unit was coupled with an electrical loading dynamometer, which allowed the engine to be tested under varying loads. The engines tested at five load levels (0%, 25%, 50%, 75% and 100%) as prepared fuel blends. Data collection and monitoring will be done in real-time using the NI USB-6210 and the Enginesoft software package. Fuel usage was determined using a 20-cc a burette along with and a stopwatch, while mass airflow was tracked using a mass airflow sensor. Emissions were measured after the engine with an AVL DiGas 444 gas analyzer and AVL 437C opacity meter. The power unitspeed during testing was kept constant, at 1500 rpm. Before data sampling, the engine was spun no-load, until a thermal steady state was reached to ensure stable combustion. For each test condition, a period was allowed for the data to stabilize. Each trial was conducted in five times under identical conditions, with the average of the five readings being recorded. The standard deviation for the repeated measures was within the accepted experimental uncertainty. The same test conditions were maintained as far as possible throughout the test campaign to minimize environmental effects. The test configuration is depicted in Fig.3, and the corresponding engine characteristics are provided in Table 6.

Table 6 Engine specification

Parameter	Details
Model	Kirolsker TV1
Engine	Four-stroke, water-cooled, Single-cylinder, CI
Rotational speed	1500 rpm
Injection pressure of fuel	210 bar
Injection time	23°bTDC
Engine rated power output	5.2 kW
Airflow	Orifice meter, U-tube manometer
Fuel Flow	Burette, Two-way cock
Dynamometer	Eddy-current dynamometer
Load Control	Electronic torque exciter (0-100%)
Speed Sensor	Flywheel-coupled
Temperature Sensor	K-type thermocouples
Cooling	Water cooling method

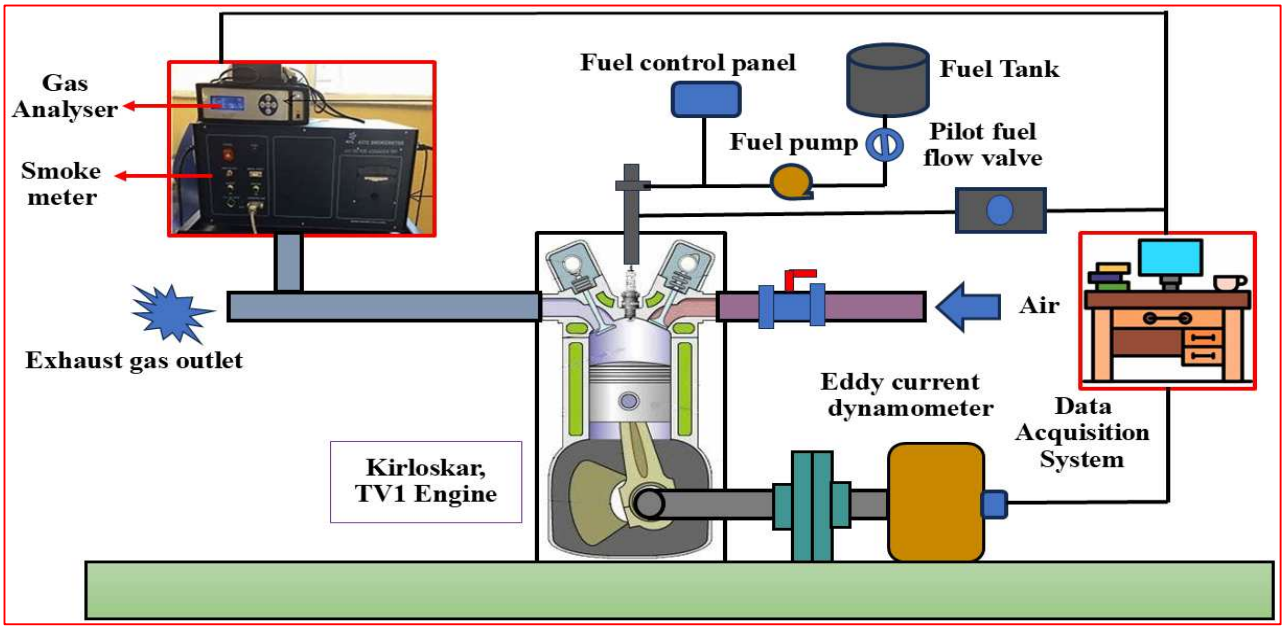


Fig.3 Schematic representation of the diesel engine experimental setup.

2.5 Uncertainty analysis of the engine

Uncertainty analysis is used to qualify experimental data of IC engines, which arise from precision and accuracy of measuring instruments, uncertainty during calibration, observable instrument resolution, environmental conditions, and the uncertainty during data acquisition. The uncertainties for the measurements were computed in accordance with the Guide to the Expression of Uncertainty in Measurement (GUM)and ISO/IEC 17025. The uncertainties of the parameters were combined as follows:

$$U_{Combined}=\sqrt{(U_{repeatability})^2+(U_{accuracy})^2+(U_{resolution})^2+(U_{precision})^2+(U_{calibration})^2}$$

Where each term reflects uncertainty arising from repeatability, instrument accuracy, resolution, precision, and calibration. The expanded uncertainty**,** representing a 95% confidence level, was computed by multiplying the combined uncertainty by a scaling factor of 2.

$$U_{expanded}=U_{Combined} \times 2$$

The uncertainty analysis was conducted to assess the reliability of the experimental data. The uncertainty of each parameter was computed in accordance with the accuracy limits of the measurement devices. The combined uncertainty was evaluated using the root-sum-square (RSS) approach, considering all measured variables involved in the calculation of performance and emission parameters. The measurement uncertainty of derived parameters, including BSFC and BTE, was obtained by considering the propagation of uncertainties from fuel consumption, load, speed, and calorific value measurements.

The total uncertainty is expressed as:

$$\text{Total uncertainty} = \sqrt{(U1^2 + U2^2 + U3^2 + \ldots + Un^2)}$$

where U denotes the uncertainty contribution of each input variable. Combined and expanded uncertainty estimates, together with their associated percentage values, are provided for every experimentally measured and analytically derived quantity. These uncertainties are displayed in their associated visual plots as bar segments, and also appear in Table 7 with expanded uncertainty and percentage values. Due to the variable conditions under which the engine tests were conducted, each engine test was repeated five times, with the results then averaged before publication. In engine testing, a margin of ±5% in reproducibility is conventionally considered acceptable.

Table 7 Uncertainty estimation of experimental parameters

Parameters	Measurement range	Instrument specification	Estimated uncertainty (%)
BP	0 -500 kW	±1% of full scale	±1%
TFC	0 - 500 kg/hr	±1% of full scale	±1%
BSFC	0.2 - 1.0 kg/kWh	Calculated parameter	±1.45%

BTE	0 – 100 %	Calculated parameter	±1.45%
Engine speed	0 - 10000 rpm	±0.003% of full scale	±0.003%
Fuel burette	0 - 500 cc	±0.01% of full scale	±0.01%
Stop watch	0 - 1000 s	±0.003% of full scale	±0.003%
Load cell	0 - 200 kg	±0.008% of full scale	±0.008%
Crank angle encoder	0 - 360°	±0.2% of full scale	±0.2%
Pressure transducer	0 - 500 bar	±0.2% of full scale	±0.2%
CO	0 – 100 %	Gas analyser accuracy ±0.3%	±0.3%
HC	0 - 1000 ppm	Gas analyser accuracy ±0.4%	±0.4%
Smoke intensity	0 - 10 HSU	Smoke meter accuracy ±0.4%	±0.4%
NO_X	0 - 1000 ppm	Gas analyser accuracy ±0.32%	±0.32%

2.6Four-ball tribometer

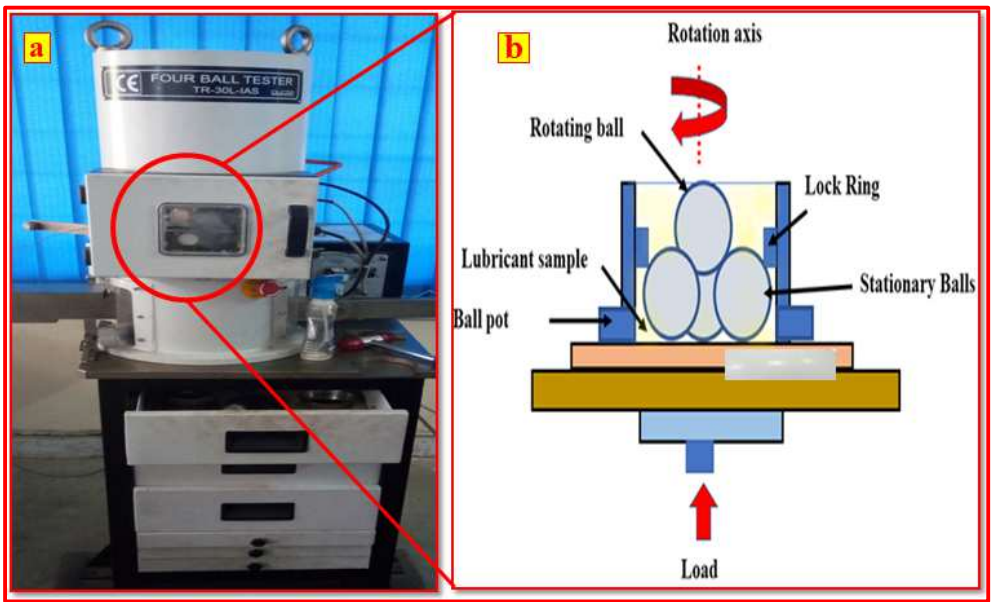


Fig.4(a) Experimental setup of the four-ball tribometer, (b) Schematic illustration of the four-ball.

Fig.4(a) Four-ball tribometer, (b) Schematic of four-ball tribometer. A ball-on-ball tribological tester (Make: Ducom Instruments, Model: TR-30L) was employedfor the friction-related study of fuel/lubricant blends by imposing different loads, speeds and temperatures under controlled experimental conditions. The tribometer consisted of a ball rolling on the collector to ensure contact with three of the balls which were fixed to the bottom of the test oil cup in a tetrahedral arrangement. The balls were tightly clamped using a wrench to the bottom of the test oil cup. The test specimens (balls) were a diameter of 0.5 inch in accordance with standard ASTM D-4172. The balls were made of chrome alloy steel in accordance with AISI E-52100 Grade 25 EP. The Rockwell hardness (C scale) was 64-66. All specimens were ultrasonically cleaned in ethanol for 5 minutes and dried with a new lint-free tissue before testing. A sample volume of 10 mL of lubricating oil was used, so that the contact area of the balls was completely covered and the friction surface was fully lubricated during the test. Testing was conducted at 40 kg load, 75 °C temperature, 1200 rpm speed and 60 minutes duration. Measurements of frictional torque were taken during the experiment. The COF was computed using Eq. (1).

$$\mu = \frac{T \times \sqrt{6}}{r \times 3w} \text{----------} 1$$

Frictional torque (T) was calculated in kg mm, where W represents the applied load in kg. The distance between the two spheres, at the point of contact, was calculated as 3.67 mm, with the shaft axis (r) as the baseline. At the conclusion of the test, the stationary balls were cleaned, The sizes of the wear scars were evaluated using an optical microscope (error ± 0.01 mm), and the wear morphology evaluated using a SEM.

2.7 Uncertainty analysis of the four-ball tribometer

The tribological tests have associated uncertainties and errors due to environmental conditions, type of equipment, test procedure, data acquisition, and calibration of sensors and instruments. Uncertainty analysis has been carried out to ensure the repeatability and reproducibility. All tribological tests were repeated three times using a four ball tribometer. The

linear approximation was employed to estimate the uncertainty in the experiments and the percentage uncertainty was found to be around ±1.884%. The accuracy and percentage uncertainty of some important tribological parameters, such as the COF and mean WSD, is summarized in Tables 8 and 9.The overall The uncertainty associated with the four-ball tribometer was evaluated using the root-sum-square (RSS) method, considering the measurement uncertaintiesassociated with the COF and WSD.

$$\text{Overall uncertainty} = \sqrt{(\text{uncertainty of COF})^2 + (\text{uncertainty of WSD})^2}$$

$$\text{Overall uncertainty} = \sqrt{(1.54657237)^2 + (2.00347853)^2}$$

$$\text{Overall uncertainty of the four-ball tribometer} = \pm 1.884\%$$

Table 8 Uncertainty analysis for the COF

Fuel samples	Trial 1	Trial 2	Trial 3	Mini mum	Maxi mum	Accuracy (±0.001)		Average	Uncertainty (%)	
						Max. +0.001 X	Min. 0.001 Y	Z= (X+Y)/2	(+) I=((X-Z)/ Z) *100	(-) I=((Y-Z)/ Z) *100
Diesel	0.169	0.168	0.167	0.167	0.169	0.17	0.166	0.168	1.19047619	-1.19047619
WPO20	0.153	0.155	0.157	0.153	0.157	0.158	0.152	0.155	1.93548387	-1.93548387
WPO20+50 ppm MgO	0.137	0.135	0.138	0.135	0.138	0.139	0.134	0.1365	1.83150183	-1.83150183
WPO20+50 ppm RuO_2	0.143	0.144	0.141	0.143	0.144	0.145	0.142	0.1435	1.04529617	-1.04529617
WPO20+50 ppm La_2O_3	0.143	0.146	0.145	0.143	0.146	0.147	0.142	0.1445	1.73010381	-1.73010381
Average uncertainty of COF									**1.54657237**	**-1.54657237**

Table 9 Uncertainty analysis for the WSD

Fuel samples	Trial 1	Trial 2	Trial 3	Mini mum	Maxi mum	Accuracy (±0.001)		Average	Uncertainty (%)	
						Max. +0.001 X	Min. 0.001 Y	Z= (X+Y)/2	(+) I=((X-Z)/ Z) *100	(-) I=((Y-Z)/ Z) *100
Diesel	0.104	0.106	0.108	0.104	0.108	0.109	0.103	0.106	2.83018868	-2.83018868
WPO20	0.0812	0.0808	0.0809	0.0808	0.0812	0.0822	0.0798	0.081	1.48148148	-1.48148148
WPO20+50 ppm MgO	0.0623	0.0626	0.0621	0.0621	0.0626	0.0636	0.0611	0.06235	2.00481155	-2.00481155
WPO20+50 ppm RuO_2	0.0656	0.0654	0.0653	0.0653	0.0656	0.0666	0.0643	0.06545	1.75706646	-1.75706646
WPO20+50 ppm La_2O_3	0.0698	0.0694	0.0691	0.0691	0.0698	0.0708	0.0681	0.06945	1.94384449	-1.94384449
Mean uncertainty in WSD									**2.00347853**	**-2.00347853**

3. Results and analysis

3.1 Classification of waste plastic oil using GC–MS analysis

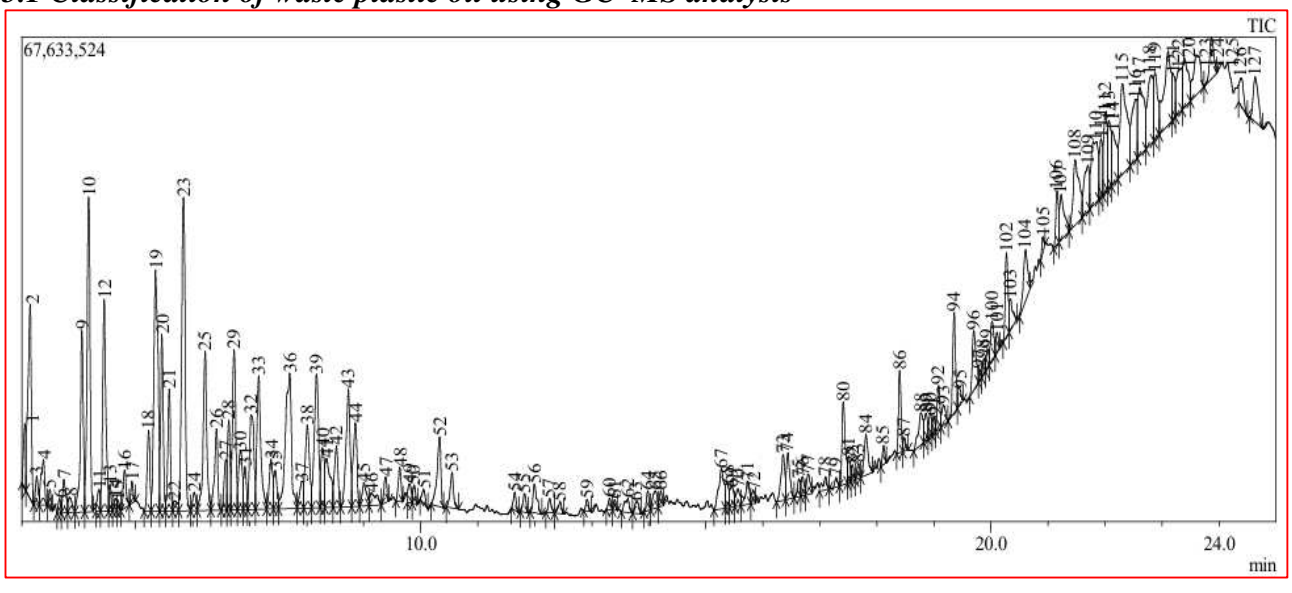


Fig.5 Compositional analysis of WPO using GC–MS

GC-MS and the corresponding chromatogram were used to analyse the chemical composition of WPO, as illustrated in Fig.5. The results reveal that WPO is a complex mixture of hydrocarbons spanning a retention time range of 3-24 minutes. At lower retention times (3 to 6 minutes), light volatile compounds, mainly light alkanes and branched hydrocarbons, were identified, corresponding to gasoline-range fractions (C5 to C12) formed during thermal degradation. In the intermediate retention range 6 to 12 minutes, a significant presence of monoaromatic hydrocarbons, including trimethylbenzene, ethylbenzene, mesitylene, indane, and tetramethylbenzene, was observed. These compounds improve calorific value and combustion stability. At higher retention times greater than 12 minutes, long-chain n-paraffins C16 to C30, such as hexadecane, eicosane, docosane, tetracosane, and triacontane, were detected, corresponding to diesel-range fractions with higher energy density. In addition, polycyclic aromatic hydrocarbons PAHs, including naphthalene and phenanthrene derivatives, were identified, which may indicate secondary cracking and recombination reactions during pyrolysis. The major compounds identified in WPO are listed in Table 10.

Table 10 Major compounds identified in WPO via GC–MS

Peak Number	Retention Time (minutes)	Compound Identification	Chemical Class	Area (%)
1	3.055	2-Pentanol, 4-methyl	Alcohol	0.60
4	3.382	Octane	Alkane	0.62
6	3.661	Decane, 2-methyl	Alkane	0.12
9–12	4.0–4.5	Cyclopentene derivatives	Cycloalkenes	2.11–3.73
18	5.225	Benzene, propyl	Aromatic	0.85
20–21	5.46–5.58	Trimethylbenzene	Aromatic	1.23–1.73
25	6.217	Mesitylene	Aromatic	2.24
26	6.417	Indane	Aromatic	1.04
36	7.701	Tetramethylbenzene	Aromatic	3.19
52–53	10.3–10.5	Naphthalene derivatives	PAHs	1.05
59	12.919	Hexadecane	Alkane	0.12
86	18.399	Heneicosane	Alkane	0.80
94	19.354	Heneicosane	Alkane	1.15
102	20.273	Docosane	Alkane	0.93
115	22.305	Triacontane	Alkane	2.52

3.2 FTIR analysis of WPO

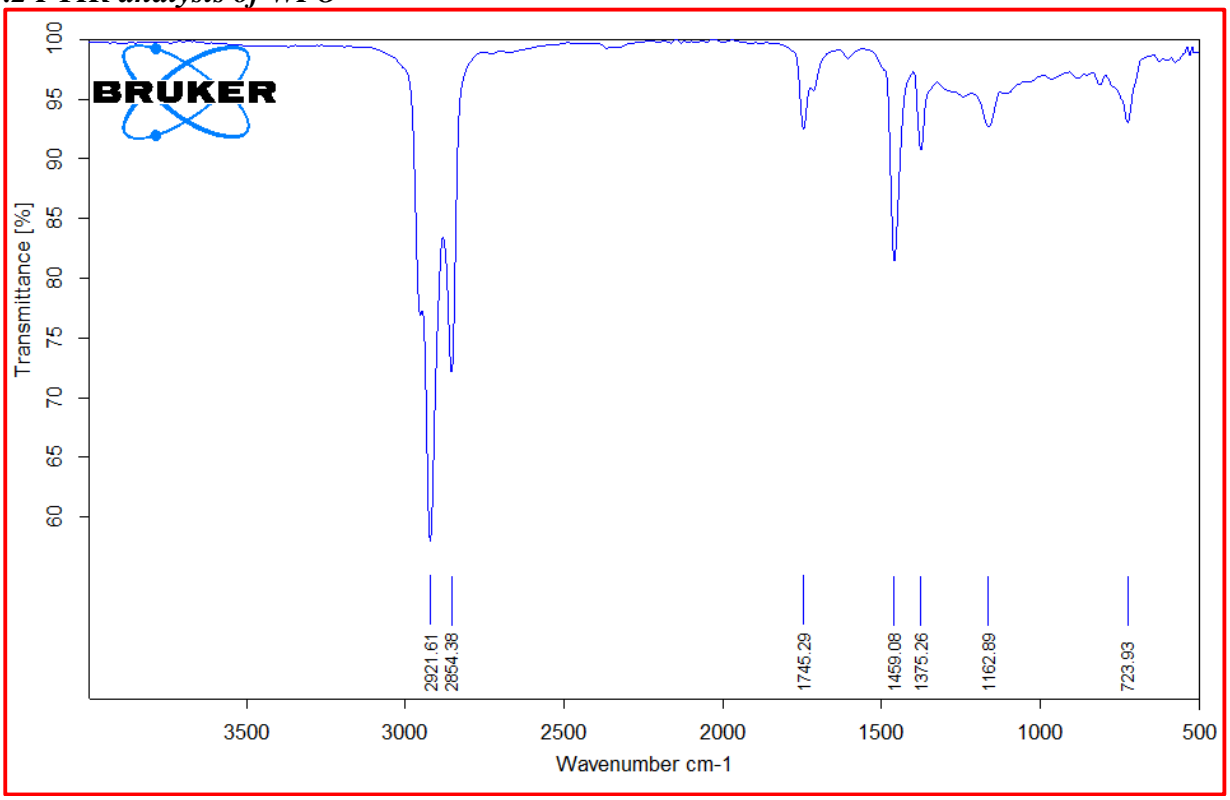
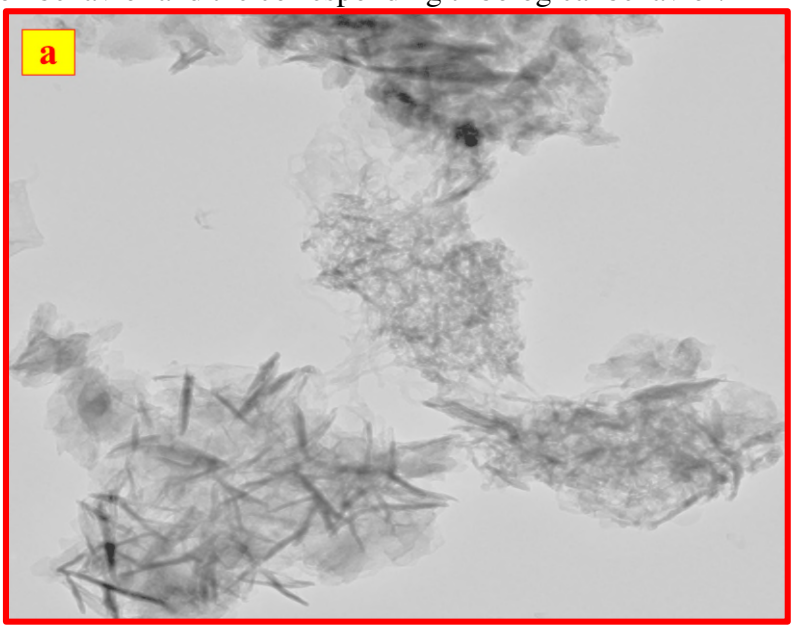


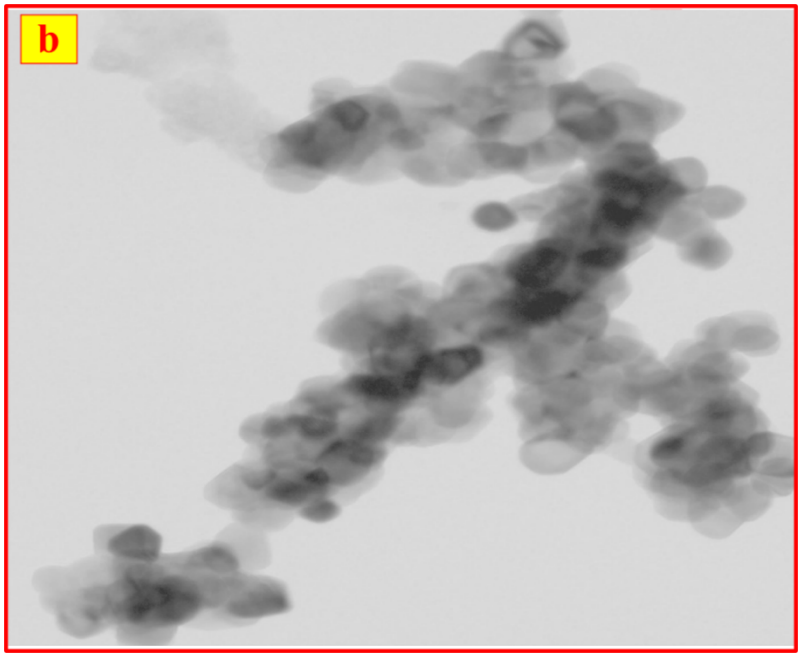
Fig.6 FTIR analysis of WPO

The FTIR spectral profile of the WPO as shown in Fig.6, the figure reveals that the functional groups associated with the degradation of plastic polymers exist in the WPO. The strong absorption band observed in the region 3000-2800 cm^{-1} corresponds to C-H stretching vibrations in alkyl groups belonging to saturated hydrocarbons, derived mainly from polyethene and polypropylene. The peak near cm^{-1} is assigned to the C=O stretching vibration of the carbonyl group compounds (ketones along withesters) formed during oxidative degradation during pyrolysis. The peak at 1600 cm^{-1} corresponds to the C=C stretching modes of the aromatic rings. It indicates the presence of aromatic hydrocarbons formed from the degradation of polymer chains. The wide absorption bands centered at about 3400 cm^{-1} resulted from O–H stretching vibration confirming hydroxyl group presence. The latter could be produced through thermal cracking and/or partial oxidation of O-H bonds. Results from FTIR spectra confirmed that WPO is a complex mixture of hydrocarbons, oxygenated products, and aromatic compounds, a typical signature of a plastic fuel product.

3.3 Microstructural characterization of nanoparticles

TEM micrograph of the MgO nanoparticles, as seen in Fig.7(a), reveals predominantly nanorod and flake-like morphologies with a primary particle size of 20–60 nm. The RuO_2 nanoparticles, as shown in Fig.7(b), are predominantly quasi-spherical and near-equiaxed in morphology, forming chain-like aggregates due to interparticle interactions, with a primary particle size of 10–40 nm, and forming larger secondary aggregates attributed to high surface reactivity and crystallinity. The nanoparticles exhibit irregular cauliflower-like clustered morphologies, as seen in Fig.7(c) for La_2O_3. The difference in the morphology observed reflects differences in surface energy, agglomeration, and particle stability, respectively, which are expected to significantly influence dispersion behavior and the corresponding tribological behavior.





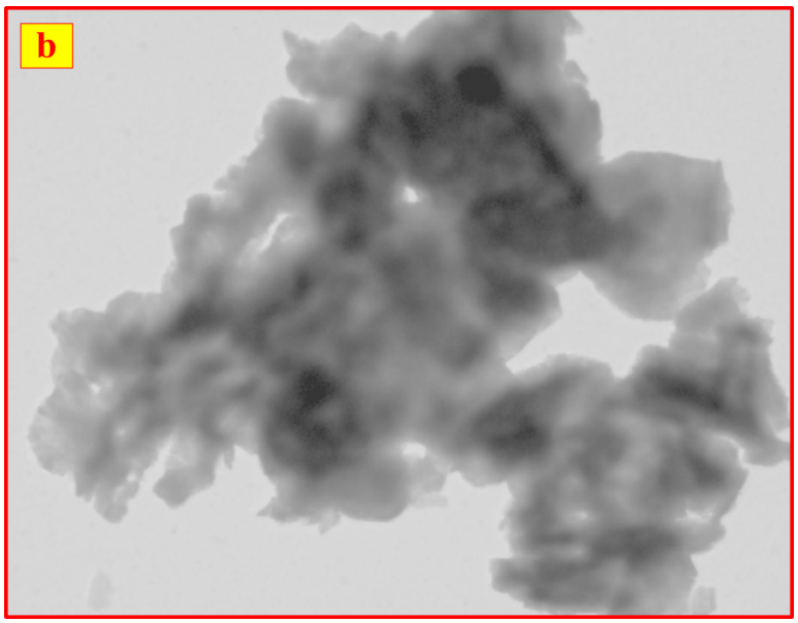


Fig.7 illustrates TEM images of (a) MgO, (b) RuO_2, and (c) La_2O_3 nanoparticles.

3.4 Impact of nanoparticles on BSFC behavior

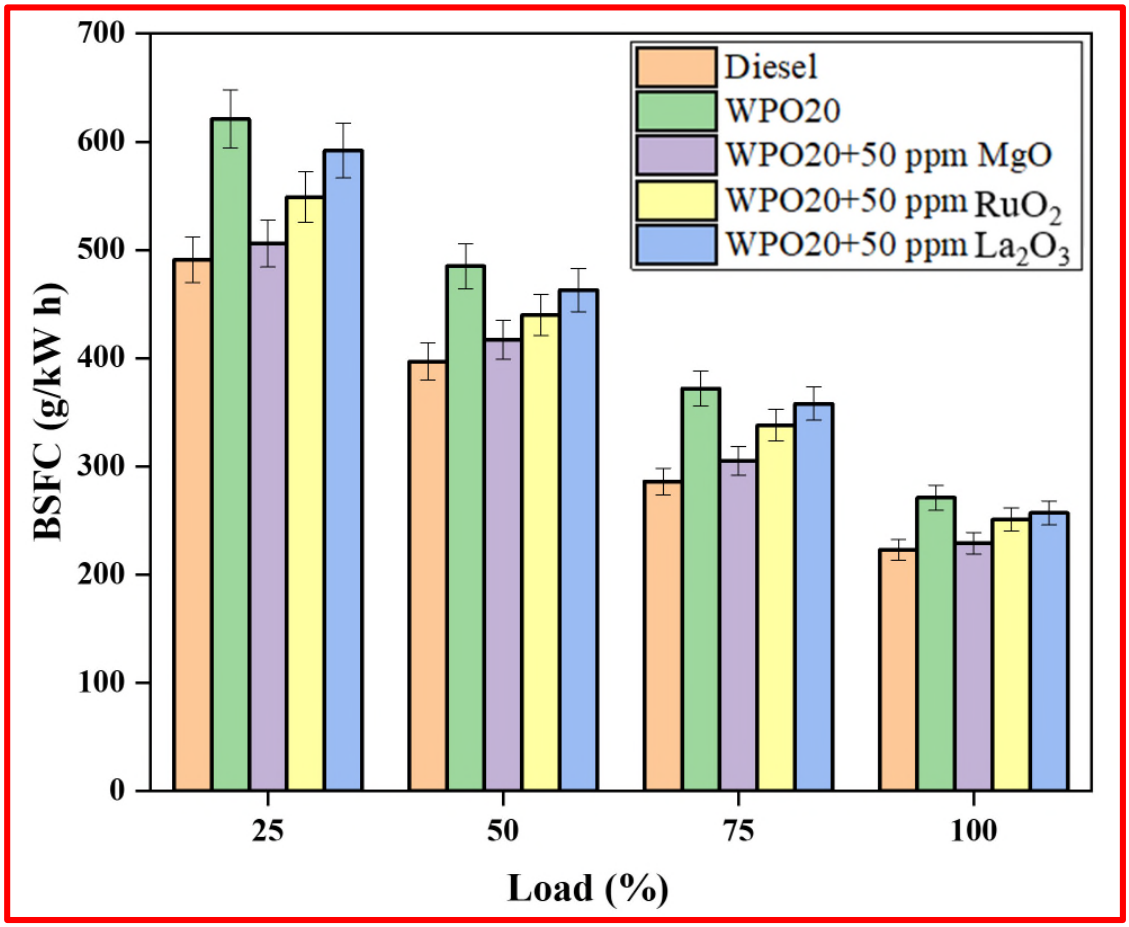


Fig.8 illustrates the effect of engine load and fuel blend on BSFC

As the power unit load increases, the fraction of usable brake power to heat losses rises, and a comparatively lower fuel quantity is required per unit of power produced. Consequently, a declining trend in BSFC was observed with increasing engine load corresponding to all tested fuels. Fig.8 illustrates the change in BSFC with nanoparticle-blended fuels under different engine loads. At peak load, the obtained BSFC values were recorded as 223 g/kWh for diesel, 271 g/kWh for WPO20, 229 g/kWh for WPO20+50 ppm MgO, 251 g/kWh for WPO20+50 ppm RuO_2, and 257 g/kWh for WPO20+50 ppm La_2O_3. It was noted that the increase in BSFC in the case of WPO20 with respect to diesel can be ascribed to the low calorific value of WPO20, which requires increased fuel supply to be injected to sustain thesame brake energy output. However, BSFC was reduced with the incorporation of nanoparticles, which improved the combustion characteristics of WPO20 fuel. The nanoparticles dispersed in this WPO20 fuel blend led to an increase in the surface area-to-volume ratio, which subsequently resulted in better catalytic activity, a shorter ignition ignition delay period, and an rise inreaction kinetics. The incorporation of nanoparticles into the fuel mixture also improved oxidation process efficiency and lowered fuel consumption at constant brake power output (Pawar et al. 2025).

3.5 Effect of nanoparticles on BTE

BTE is significantly affected by combustion characteristics, oxygen availability, and air–fuel mixing. Fig.9 shows the BTE for the different fuel blends under various engine loads. The BTE of all fuels rises with increasing engine load, due to better combustion and reduced relative heat losses with increased load condition of the engine. Under highest engine load, the BTE values were found to be 32.47% for diesel, 30.54% for WPO20, 31.62% for WPO20+50 ppm MgO, 31.15% for WPO20+50 ppm RuO_2, and 31.02% for WPO20+50 ppm La_2O_3. The lower BTE of WPO20 fuel can be related to its low calorific value, high viscosity, density and flash point, which lead to improper fuel dispersion and air–fuel mixing quality, and consequently, poor combustion and lower thermal conversion efficiency. In contrast, nanoparticles added to WPO20 fuel were shown to improve the BTE as a result of improved combustion behavior. Due to their high surface-to-volume ratio, nanoparticles improve oxidation reactions via catalytic effects and improved oxygen availability during combustion, resulting in improved air–fuel blending and additional factors efficient fuel utilization. Further, the nanoparticles dispersed fuel blends may influence fuel spray evaporation characteristics and ignition delay times, and therefore also improve the rate of

heat release and the combustion efficiency (Jathar et al. 2025). WPO20+50 ppm MgO gave the highest value of BTE of all the mixtures.

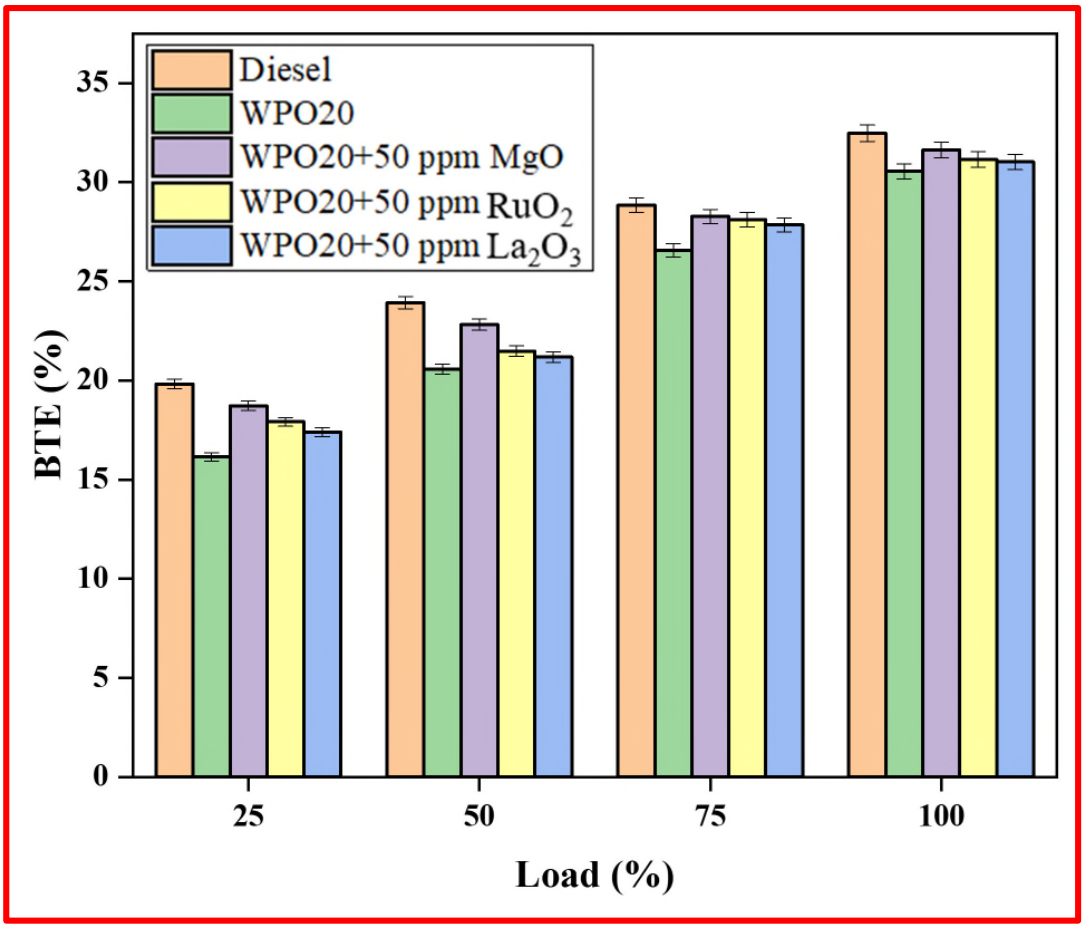


Fig. 9 depicts the effect of engine load and fuel mixture on BTE.

3.6 Effect of nanoparticles on CO emissions

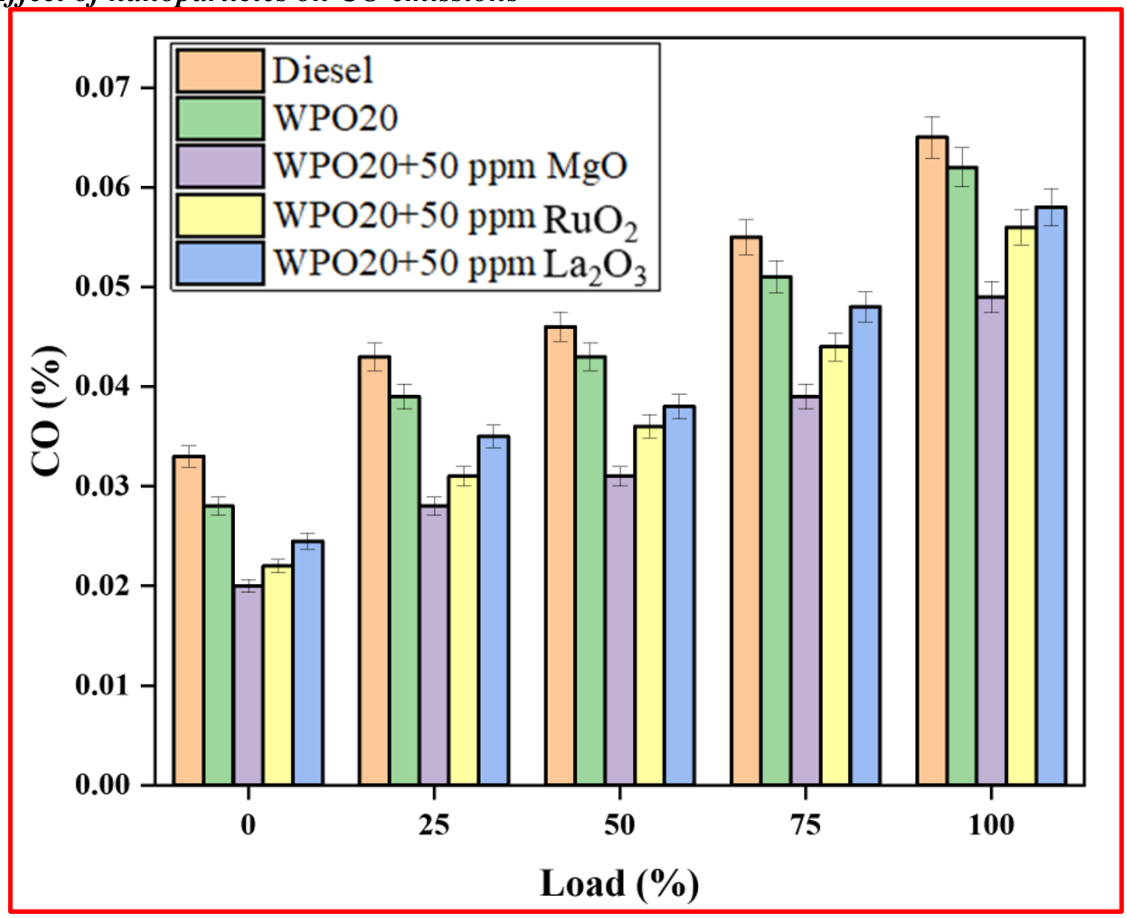


Fig.10 depicts the effect of engine load and fuel composition on CO emissions.

CO is primarily formed as a consequence of incomplete fuel oxidation under rich mixture conditions. The effect of engine load on the emission of CO is shown for different nanofuel blends

in Fig.10. At maximum load, CO emissions were measured as0.065%, 0.062%, 0.049%, 0.056%, and 0.058% for diesel, WPO20, WPO20+50 ppm MgO, WPO20+50 ppm RuO_2, and WPO20+50 ppm La_2O_3, respectively. According to the results, the WPO20 fuel mixturereduce the CO emission, compared with diesel, due to the higher proportion of intrinsic oxygen and oxidative property of the waste plastic oil-based fuel, promoting enhanced combustion efficiency ata high load. However, the blended fuel still experiences incomplete combustion resulting from inhomogeneous spray formation and elevated viscosity. In contrast, the addition of nanoparticles further reduced CO emissions in comparison with diesel and WPO20 blends. This decrease ismainly ascribed to the catalytic activity of nanoparticles, which enhances surface-mediated oxidative reactions andimproves the transformation of carbonaceous intermediates (CO and HC) into CO_2. In addition, improved spray characteristics and enhanced air–fuel mixture formation promote more complete combustion, thus reducing the generation of incomplete combustion products (Karthikeyan et al. 2026). Among all evaluated fuels, WPO20+50 ppm MgO exhibited the lowest CO emissions.

3. Influence of nanoparticles on Hydrocarbon (HC) emissions

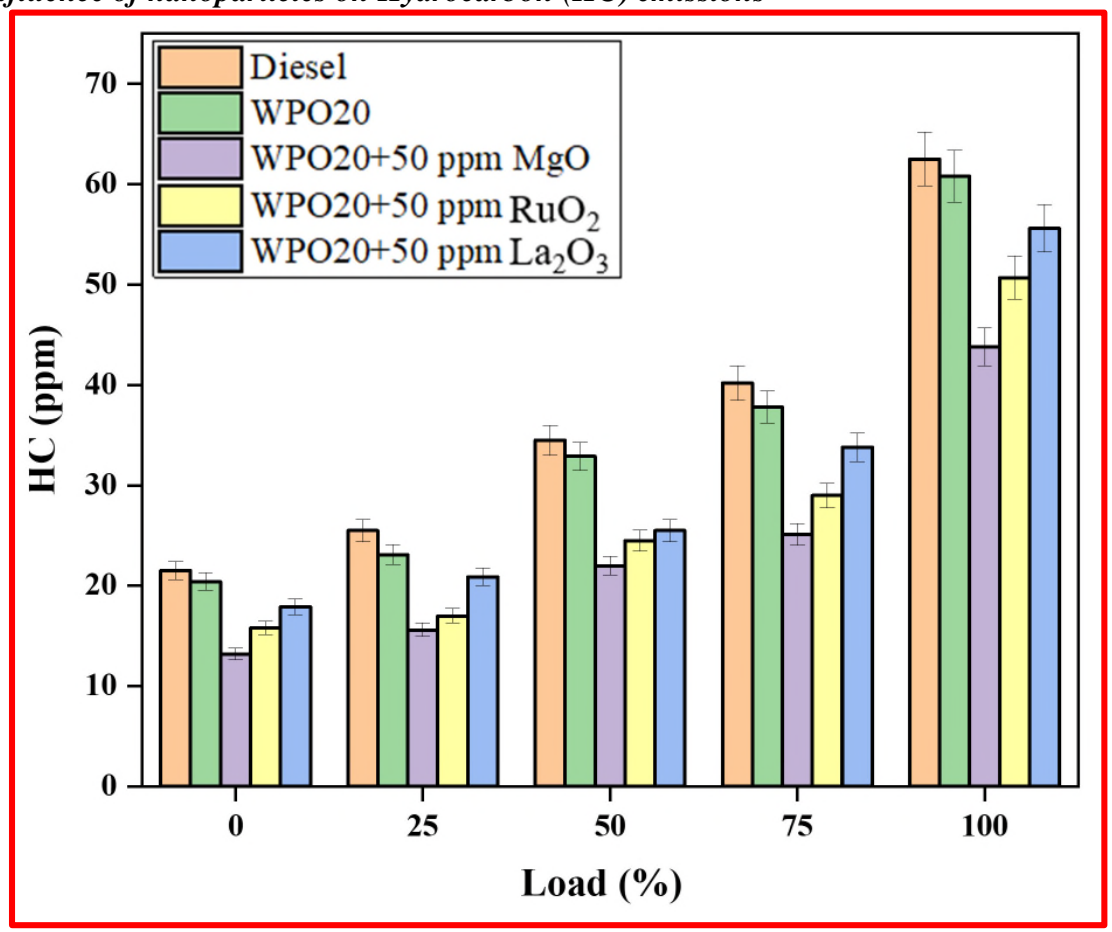


Fig. 11 illustrates the change in HC with various engine load conditions and fuel mixtures.

HC emissions rose with increasing engine load across all tested fuel blends, reaching their highest values at full load. Fig.11 depicts the variation in HC emissions as a function of engine operating conditions and load for diesel, WPO20, and WPO20 blended with various nanoparticles. At peak load, HC emissions were measured as 62.5 ppm for diesel, 60.8 ppm for WPO20, 43.8 ppm for WPO20+50 ppm MgO, 50.7 ppm for WPO20+50 ppm RuO_2, and 55.6 ppm for WPO20+50 ppm La_2O_3. The HC emissions from WPO20 in the current study were were lower than diesel because of improved combustion characteristics of the WPO20 blend from the oxygenated fuel components it contains. The incorporation of nanoparticles into the WPO20 reduced the HC emissions due to faster oxidation, which leads to more complete burning of unburned hydrocarbons. This effect has been ascribed to the catalytic activity of nanoparticles, thereby promoting formation of reactive oxygen species, enhance fuel reactivity, shorten the ignition delay period and improve combustion quality, resulting in complete fuel oxidation during both the premixed and diffusion combustion phases. Moreover, improvements in fuel atomization, atomized fuel spray structure and the air-fuel mixture caused by the presence of nanoparticles enhances combustion uniformity and decreases HC emissions (Mulk et al. 2026).

3.8 Effect of nanoparticles on smoke opacity

At full load, smoke opacity increases owing to increased fuel consumption, injection rates, and reduced time available to achieve complete combustion. Inadequate air–fuel mixing contributes to incomplete combustion, leading to increased smoke formation. Fig.12 demonstrates how smoke opacity varies across the load under different fuel conditions and blends. During maximum load operation, the smoke density was determined to be 61.8% for diesel, 59.6% for WPO20, 51.4% for WPO20+50 ppm MgO, 54.8% for WPO20+50 ppm RuO_2, and 58.36% for WPO20+50 ppm La_2O_3. The WPO20 blend also led to increased smoke opacity compared with nanoparticle-containing fuels due to its relatively elevated viscosity and lower volatility, resulting in poorer atomization. Furthermore, due to the larger droplet size, leading to slower evaporation and localized fuel accumulation during the diffusion combustion stage, promoting soot formation. The presence of nanoparticles in WPO20 resulted in reduced smoke formation by improving combustion, catalyzing the oxidation of hydrocarbons and soot precursors, reducing soot and particulate formation. Conversely, the high surface energy of the nanoparticles and the presence of catalytic active sites give rise to micro-scale combustion and accelerate the oxidation of intermediate carbon species. Improved atomization of the nanoparticle-doped fuel and better dispersion of nanoparticles within the fuel promotes improved air–fuel mixing and less soot-rich fuel-rich zones. With the increase in nanoparticle concentration, oxidation of soot, along with improved combustion kinetics, contributes to reduced smoke opacity (Zafar et al. 2026).

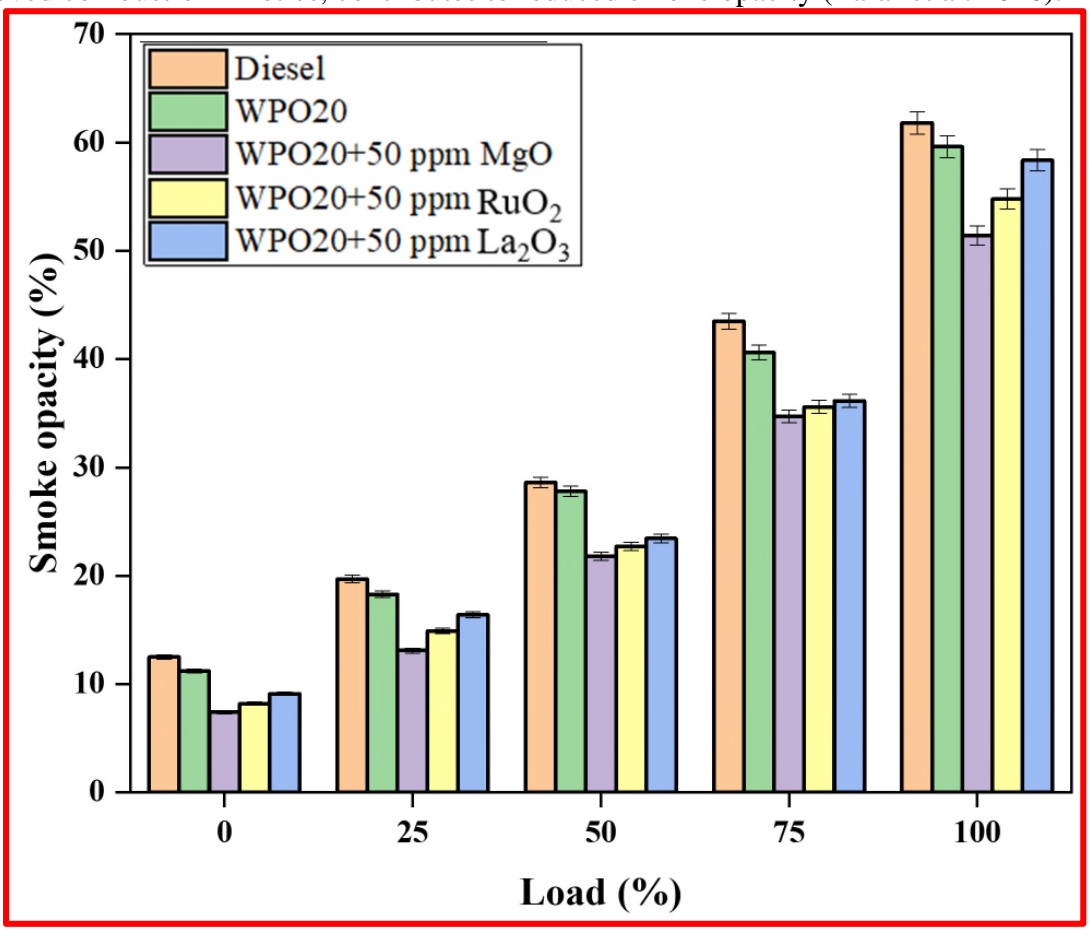


Fig.12 illustrates the smoke density trends with varying engine loads and fuel blends.

3.9 Influence of nanoparticles on NOx emissions

The NO_X emissions are quite low at the minimum load, but increase at higher load, caused by elevated engine combustion temperature. The generation of NOx depends very strongly on the flame temperature during combustion, which increases with the increase of the ignition rates at higher load. The change in NOx emissions in relation to respect to engine load under pure diesel, WPO20, and WPO20 mixed with various nanoparticles is shown in Fig.13. At peak load, NO_X emissions were measured as1509 ppm for diesel, 1515 ppm for WPO20, 1622 ppm for WPO20+50 ppm MgO, 1576 ppm for WPO20+50 ppm RuO_2, and 1563 ppm for WPO20+50 ppm La_2O_3. The elevated NOx emissions observed with the WPO20 and the nanoparticle blends compared with diesel can be explained by the fuel properties related to the oxygenated nature of the WPO molecule, which contributes to an increase in local flame temperature and combustion

quality, thus increasing NO_X emissions. The nanoparticles have also been used as combustion catalysts resulting from their high surface area, which improves fuel-oxygen contact and oxidation. This contributes to reduced ignition delay and may advance combustion phasing, increasing the premixed combustion fraction and contributing to higher peak in-cylinder temperatures. Additionally, higher temperatures also increase formation of thermal NOx via the Zeldovich thermal NOx mechanism. Nanoparticle addition improves the atomization and dispersion of fuel droplets within the combustion chamber, leading toa more homogeneous air-fuel blend with improved localized heating. This catalytic activity was strengthened in samples with high nanoparticle concentrations, increasing the flaming region temperature in the combustion chamber (Modi et al. 2024). Therefore, the oxygen enrichment, catalytic action, and improved combustion kinetics increased the NO_X emissions in both WPO20 and its nanoparticle blends compared to pure diesel.

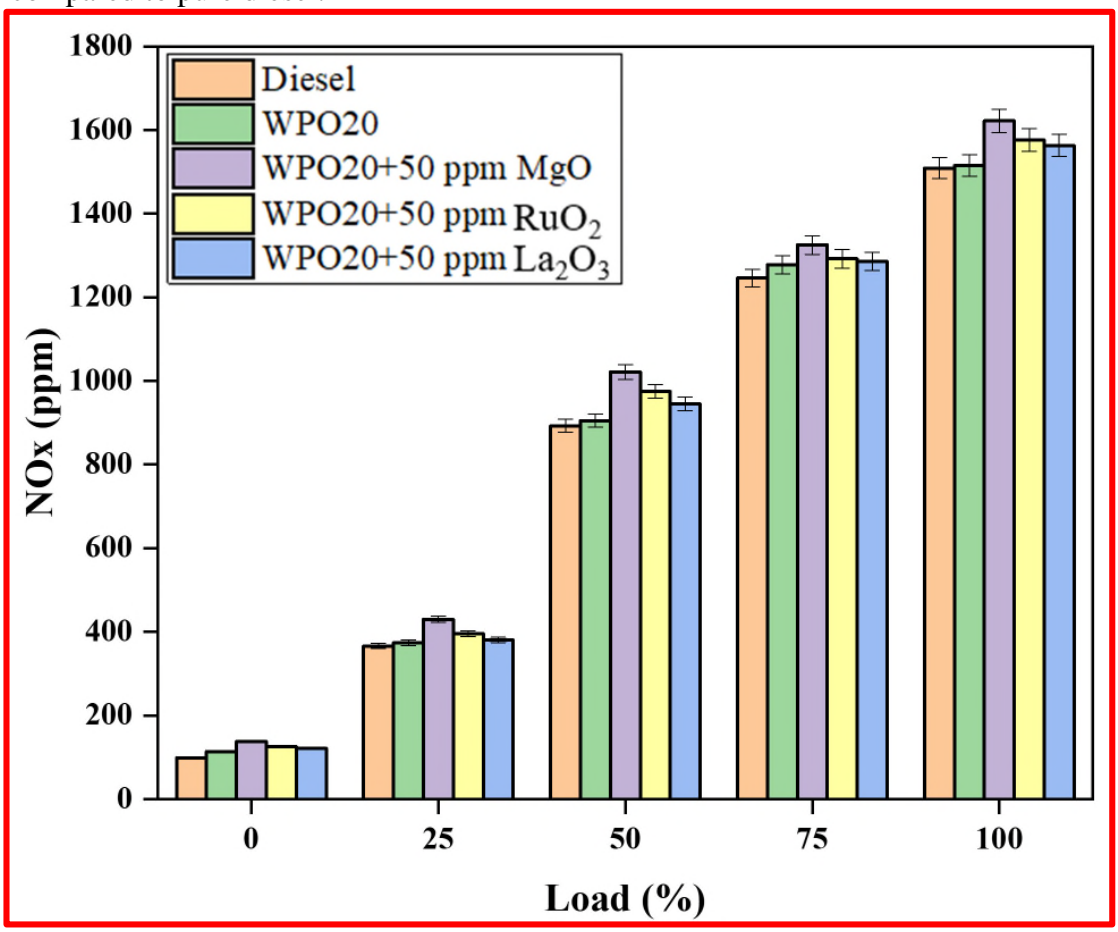


Fig. 13 shows the variation of NOx emissions with engine load for the tested fuel blends.

4. Tribology characteristics

4.1 Influence of nanoparticles on the COF

The tribological tests were repeated thrice for each fuel blend and average COF and WSD were reported. The variation of COF using different fuel blends is shown in Fig.14. Higher COF is associated with poor lubricating film strength and increased metal–metal interaction, and less separation of the surfaces. The COF for diesel, WPO20, WPO20+50 ppm MgO, WPO20+50 ppm RuO_2 and WPO20+50 ppm La_2O_3 were 0.169, 0.157, 0.138, 0.144, and 0.146 respectively. This indicates that diesel oil had a higher COF than WPO20. The superior COF performance of WPO20 compared to diesel oil could be due to the heavy hydrocarbon fractions and polar compounds that were formed during the pyrolysis of waste plastic to give better boundary lubrication between the friction surfaces and the thin lubricating film. The addition of nanoparticles lowered the COF values due to their high dispersion stability, enhanced load-carrying capacity, and improved tribofilm formation and stability at the contact interface (Gupta et al. 2024).The tribofilm reduces direct asperity contact and shear resistance. The WPO20+50 ppm MgO sample showed the lowest COF value.

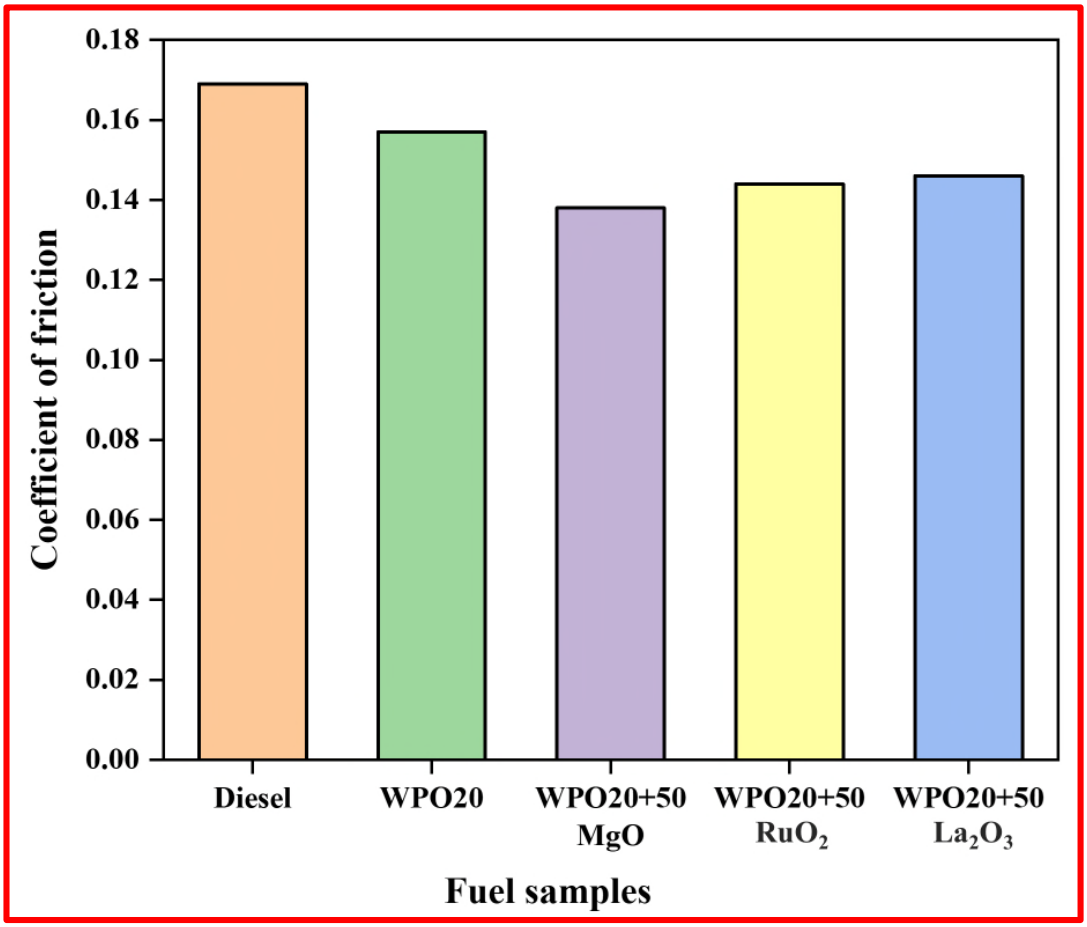


Fig.14 illustrates COF trends across various fuel blends

4.2 Effect of nanoparticles on WSD

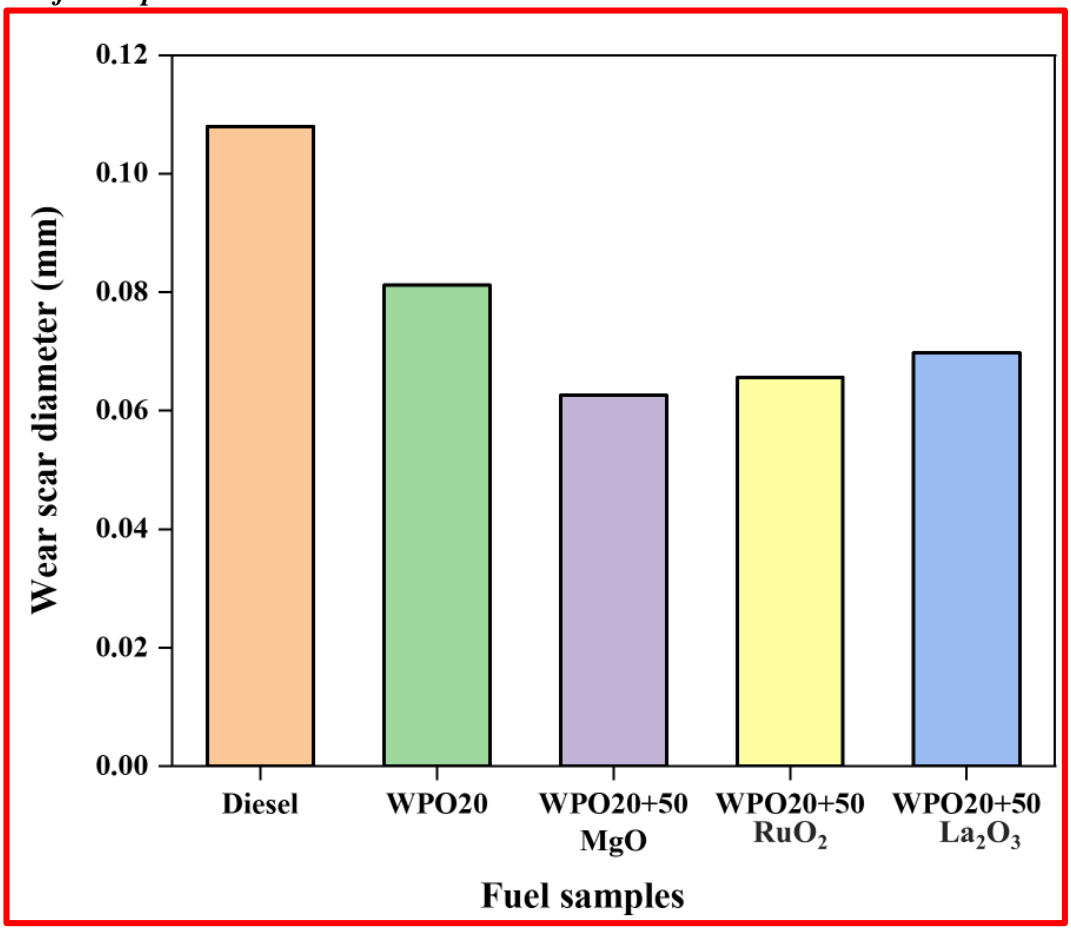


Fig. 15 highlights WSD variation across different fuel blends.

The WSD is inversely correlated with COF. The WSD values of diesel, WPO20, WPO20+50 ppm MgO, WPO20+50 ppm RuO_2 and WPO20+50 ppm La_2O_3 were shown to be 0.108 mm, 0.0812 mm,0.0626 mm, 0.0656 mm and 0.0698 mm respectively as shown in Fig.15.

The WSD of WPO20 blend is lower than that of diesel because of heavy hydrocarbon fractions and polar oxygenated compounds in WPO which help to provide better boundary lubrication through the formation of a partial interfacial film between thecontacting metallic interfaces and reducing the direct contact area between the surfaces, thereby reducing wear. Furthermore, the addition of nanoparticles into the WPO20 formulation also decreased the WSD through several synergistic tribological mechanisms. These mechanisms include the generation of a stable tribo-protective layer on theworn surfaces, the mending impact during the friction process, where nanoparticles fill surface asperities and microvalleys of the material surface, and the load-carrying effect, which reduced the contact pressure (Ravikiran et al. 2025). The rolling and polishing action of the well-dispersed nanoparticles reduced WSD further. WPO20+50 ppm MgO had the lowest WSD of all the samples, and thus its better tribological characteristics were attributed to the increased nanoparticle concentration, which promoted better lubrication, surface coverage, and stable third-body lubrication, and reduced adhesive wear and abrasive wear. These results indicated that incorporating nanoparticles enhances the tribological performance of the WPO20 blend.

4.3 Surface morphology of tribo-test specimens by using SEM analysis

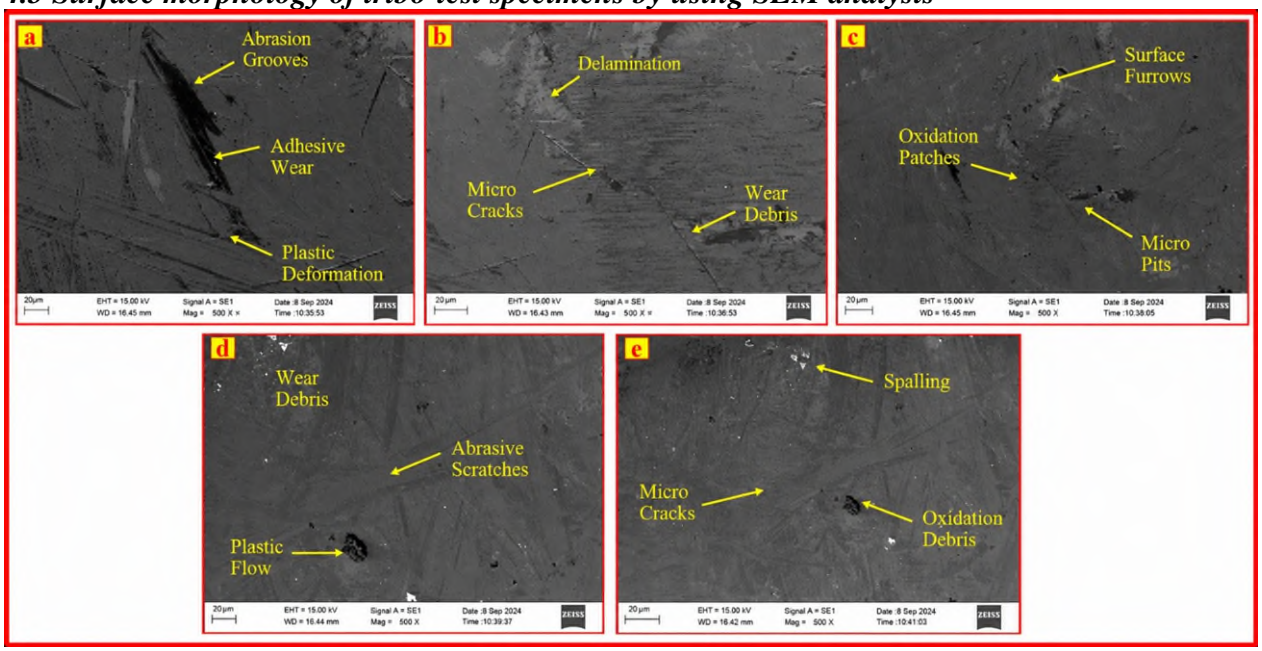


Fig.16 SEM analysis of wear-affected surfaces of tested balls under varying lubrication conditions: (a) diesel, (b) WPO20, (c) WPO20+50 ppm MgO, (d) WPO20+50 ppm RuO_2, and (e) WPO20+50 ppm La_2O_3

The worn surface morphologies under various lubrication conditions are displayed in SEM micrographs, as shown in Fig.16(a–e). The surface characteristics were studied to understand the impact of fuel composition and the addition of nanoparticles on the tribological behavior and associated wear mechanism. The surface of the sample taken from the diesel-lubricated condition is shown in Fig.16(a) and shows severe surface damage in the form of deep abrasion grooves, adhesive wear regions, and plastic deformation along the direction of sliding. The surface defects are attributed to high asperity interaction, high contact stress on the contacting surfaces, and the lack of formation of a protective lubricating layer, increasing the material removal from the contacting surfaces. For the WPO20 lubricated sample as shown in Fig.16(b), the surface morphology is better than that of the sample lubricated by diesel; the groove depth is less, and the grooves on the wear track are relatively smooth (Yilmaz et al. 2025). On the other hand, the delamination, micro-cracks, and wear debris observed suggest that there is surface fatigue and detachment of material due to the limited stability of the protective tribofilm during sliding.

Fig.16(c) shows the surface integrity after adding MgO nanoparticles to WPO20, which was greatly improved. The surface is eroded, and the amount of severe damage features is reduced; only minor surface furrows, oxidation patches, and micro-pits are visible. The tribological contribution of the MgO nanoparticles contributes to enhanced wear resistance. The high hardness and chemical stability ensure that the MgO nanoparticles have the ability to withstand the contact load applied and minimize the direct interaction between metallic asperities. Due to their nanoscale dimensions, they can enter surface valleys and irregularities and create a nano-rolling effect that

facilitates sliding and minimizes frictional resistance. Moreover, the nanoparticles of MgO create a stable oxide-based tribofilm, which serves as a protective barrier and reduces the adhesive and abrasive wear mechanisms. The RuO_2 blend shown in Fig.16(d) has better surface protection than the WPO20, but abrasive scratches, wear debris, and plastic flow regions can still be observed. Therefore, the lubrication behaviour is improved due to the formation of a protective surface layer in the presence of RuO_2 nanoparticles, but minor surface damage is still observed in the form of mild scratches, resulting from local particle agglomeration and from the lack of particle coverage over the surface. Similarly, WPO20 with La_2O_3 as presented in Fig.16(e), which exhibits lesser severity of wear than the base fuel; however, the presence of microcracks, spalling, and oxidation debris suggests the presence of fatigue and oxidation-assisted wear mechanisms during sliding. The SEM results are in agreement with the tribological results of the tested samples. Based on the results of all the additives investigated, the surface protection ability of MgO was the most effective, where it reduced abrasive and adhesive interaction by rolling effect, the surface-filling effect, and the ability to form a protective tribofilm. Better morphology of wear debris indicates the improvement of lubrication stability and wear resistance of WPO20 loaded with MgO nanoparticles under sliding contact conditions.

5. Comparison of current results with previous studies

The performance, emission, and tribological properties of WPO20 fuel containing MgO, RuO_2, and La_2O_3 nanoparticles (50 ppm) were carefully examined and compared with baseline WPO20 fuel, as shown in Table 11. From the engine and tribology analysis, the WPO20+50 ppm MgO blend was better than those of other reported WPO blends. This improvement is ascribed to the following: better burning process properties, more oxygen available, and catalytic properties of nanoparticles, which lead to enhanced combustion completeness and decreased incomplete combustion products. Further, the presence of nanoparticles on rubbing surfaces allows the development of a well-developed protective tribofilm that helps to decrease friction and wear. The findings of the current experimental investigation have been summarized and compared with the existing studies in Table 12.

Table 11 reports the percentage variations relative to the baseline fuel, where a (+) sign denotes an increase and a (−) sign denotes a decrease in the corresponding parameters.

Rate of change	WPO20+50 ppm La_2O_3 (%)	WPO20+50 ppm RuO_2 (%)	WPO20+50 ppm MgO (%)
BSFC	−5.17	−7.38	−15.5
BTE	+1.57	+2	+3.53
CO	−6.45	−9.68	−20.97
HC	−8.55	−16.45	−27.96
Smoke Opacity	−2.08	−8.05	−13.76
NO_X	+3.17	+4.03	+7.07
COF	−7.01	−8.28	−12.1
WSD	−14.29	−19.21	−22.9

Table 12 Assessment of performance and emission characteristics of the present study with respect to existing literature

References	Optimum blend	Reference sample	BSFC (%)	BTE (%)	CO (%)	HC (%)	Smoke (%)	NO_X (%)	COF (%)	WSD (%)
(Soundararajan et al. 2025)	ULDP20G40	ULDP20	-6.85	+5.71	-7.04	-3.71	-2.33	-1.63	-	-
(Suhel et al. 2023)	WPO15ZnO100	WPO15	-12.8	+2.47	-5.7	-28	-11.8	-14.9	-	-
(Sachuthananthan et al. 2021)	PPO+75MNA	PPO	-12.5	+7.93	-	-4.28	-11.9	+3.06	-	-
(Sundar et al. 2022)	POAL200	PO	-	+2.6	-45.4	-18	-	+5.2	-	-

(Thomas et al. 2022)	PAN200	PO	-9.1	+10.3	-55.6	-62.3	-33	-7.7	-	-
(Thilipkumar et al. 2026)	SAME20 + 90 ppm GO	SAME20	-13.6	+3.79	-23.8	-22.8	-8	+10.4	-16.2	-30.4
At present study	WPO20+50 ppm MgO	WPO20	-15.5	+3.53	-20.97	-27.96	-13.76	+7.07	-12.1	-22.9

6. Conclusion

The current study investigates the influence of MgO, RuO_2, and La_2O_3 nanoparticles on the performance, emission, and tribological Features of a CI engine operated using WPO blends. Five fuels were prepared and tested: diesel, WPO20, WPO20+50 ppm MgO, WPO20+50 ppm RuO_2, WPO20+50 ppm La_2O_3. The tribological performance of the fuel blends was tested on a four-ball tribometer. The conclusions based on those tests are given below.

- The characterization of nanoparticles was performed using TEM, which provided detailed information on particle size distribution.
- At peak engine load, the brake thermal efficiency was enhanced by 3.41%, and the BSFC was decreased by 15.05% for the WPO20+50 ppm MgO blend in comparison to WPO20 , mainly due to the enhancement in the oxygenation and combustion properties of the nanoparticles.
- Under full-load conditions, the WPO20+50 ppm MgO blend resulted in 20.97%, 27.96% and 13.75% decreases in CO, HC, and smoke emissionsopacity emission concentrations respectively. The only increase was in the NO_X emission by 6.5% due to the rise in in-cylinder combustion temperature, which results in a reasonable rise in the oxidative reactions within the combustion chamber.
- Tribological tests revealed that the lubricant with WPO20+50 ppm MgO was better than the base fluid, as the COF was decreased by 29.5% and WSD by 30%.SEM micrographs of worn surfaces of WPO20 with nanoparticles reduced the grooves, metal extrusions, and the degree of roughness of the surfaces in contact with diesel and WPO20, exhibiting better anti-wear and protecting tribofilms formation performance.

Therefore, the overall results of the present experimental investigation show that La_2O_3 nanoparticle-assisted WPO blends can serve as an alternative fuel to CI engines with improved combustion behavior, reduced emissions, and improved tribological performance. The best performance was observed for the blend WPO20+50 ppm MgO.

6.1 Limitations of the present study

Limitations of this study were that the extended-term dispersion stability along with long-term storage stability and dispersion behavior of nanoparticles within WPO blends were not extensively studied, tests were not carried out under different engine operating parameters such as injection pressure, injection timing, and speed variations and wear tests over prolonged engine operation were not conducted. However, the majority of the emissions were reduced to a large extent, with a a marginal increase in NO_X emissions, and further optimization strategies are required to minimize NO_X emissions**.**

6.2 Future scope

Thus, continuing research in this field should be focused on the dispersion stability and storage properties of the nanoparticles blended with WPO, as well as on long-term engine durability/tribological behavior studies at operating conditions, to assess the long-term viability of the fuel blends. Future tests should also assess the influence of injection pressure, injection timing, and crank angle on engine efficiency. Other techniques such as EGR, SCR and water emulsification can be used in conjunction with the nanoparticle assisted WPO fuels in CI engines to reduce NO_X emissions. More investigation is needed tostudy the practicality ofthese fuels for commercialization.

7. Reference

Afroze CA, Ahmed MN, Azam MNK, Jahan R, Rahman H. “Microplastics pollution in Bangladesh: A decade of challenges, impacts, and pathways to sustainability.” *Integrated Environmental Assessment and Management.* 2026;22(1):98–115. https://doi.org/10.1093/inteam/vjaf108

Ahmad A, Yadav AK, Hasan S. A novel waste-to-energy conversion plant based on catalytic pyrolytic conditions: modeling and optimization using supervised machine learning and

desirability-driven methodologies. *Energy*. 2025;317:134648. doi:10.1016/j.energy.2024.134648. https://doi.org/10.1016/j.energy.2025.134648

Anand T, Debbarma S. Performance and emission characteristics of a CRDI diesel engine operated on waste plastic oil with hydrogen enrichment under variable injection parameters. *Int J Hydrogen Energy*. 2026;215:153874. doi:10.1016/j.ijhydene.2024.153874. https://doi.org/10.1016/j.ijhydene.2026.153874

Baskar S, Arumugam S, Sriram G, Sistla VSSS. Tribological investigation of waste plastic oil-based methyl ester blended synthetic lubricant using four-ball tribometer. In: *Advances in Materials and Manufacturing Engineering (ICMME 2019 Proceedings)*. 2019:587-593.https://doi.org/10.1007/978-981-15-6267-9_66

Burra KR, Sahin M, Zheng Y, Gupta AK. Near-critical CO_2-assisted liquefaction-extraction of biomass and wastes to fuels and value-added products. *J Energy Res Technol*. 2024;146(1):011801. DOI: https://doi.org/10.1115/1.4063813

Canan A. Multi-purpose optimization with response surface methodology of plastic waste cables to clean energy with graphene nanoparticles. *J Environ Manage*. 2025;391:126336. https://doi.org/10.1016/j.jenvman.2025.126336

Das AK, Mohapatra T. Exergetic performance optimization and thermoeconomic analysis of a variable compression ratio diesel engine fueled with distilled plastic oil and diesel doped with nanographene. *Proc Inst Mech Eng Part E: J Process Mech Eng*. 2024:09544089241229563.https://doi.org/10.1177/09544089241229563

Deepankumar S, KL SK. Extraction and characterization of pyrolysis oil from e-waste plastics with SiO_2 nano-additives for enhanced performance in CI engines. 2025. https://doi.org/10.21203/rs.3.rs-6319906/v1

Drobne D, Ambrožič Avguštin J, Kralj MB, Čehovin Zajc J, Čremožnik Zupančič J, Dragoš A, Ficko A, Fišer C, Bulc TG, Heath E, Hočevar M. Microbiome: a nexus of One Health strategies to address emerging risks. *BioScience*. 2026:biag011. https://doi.org/10.1093/biosci/biag011

Gnanamoorthi V, Murugan M. Effect of DEE and MEA as additives on a CRDI diesel engine fueled with waste plastic oil blend. Energy Sources, Part A: Recovery, Utilization, and Environmental Effects 2022;44(2):5016–5031.https://doi.org/10.1080/15567036.2019.1657206

Gupta HS, Sehgal R, Wani MF. Tribological characterization of eco-friendly bio-based mahua and flaxseed oil through nanoparticles. *Biomass Conv Bioref*. 2024;14(10):11251-11263. https://doi.org/10.1007/s13399-023-04597-1

Januszewicz K, Hunicz J, Kazimierski P, Rybak A, Suchocki T, Duda K, Mikulski M. "An experimental assessment on a diesel engine powered by blends of waste-plastic-derived pyrolysis oil with diesel." *Energy*. 2023;281:128330.https://doi.org/10.1016/j.energy.2023.128330

Jathar LD, Meherunnesa, Shelare S, Shahapurkar K, Abedin T, Farade RA, Rajabi A, Khan TMY, Singh R, Cuce E, Nur-E-Alam M. "A short review on nano-additives to enhance biodiesel performance in diesel engines." *Journal of Thermal Science*. 2025;34(4):1450–1473. DOI: https://doi.org/10.1007/s11630-025-2080-y

Karthikeyan MA. A state-of-the-art review on the application of nanotechnology in biodiesel blends: exploring the thermo-chemical interactions, performance improvements, and ecotoxicological aspects. *Environmental Progress & Sustainable Energy*. 2026:e70390. doi:https://doi.org/10.1002/ep.70390

Karthikeyan S, Prabhakaran TD, Prathima AJE. Environmental effect of La_2O_3 nano-additives on microalgae-biodiesel fueled CRDI engine with conventional diesel. *Energy Sources Part A*. 2018;40(2):179-185.https://doi.org/10.1080/15567036.2017.1407843

Kumar KS, Muniamuthu S. Assessment of performance, combustion, and emission characteristics of single cylinder diesel engine fuelled by pyrolysis oil + CeO_2 nanoparticles and 1-butanol blends. *Int J Ambient Energy*. 2024;45(1):2344568.https://doi.org/10.1080/01430750.2024.2344568

Livingston TS, Madhu P, Dhanalakshmi CS, Kumar RV. An experimental investigation on performance, emission and combustion characteristics of IC engine using liquid fuel produced through catalytic co-pyrolysis of pressed oil cake and mixed plastics with the addition of nanoparticles. *Fuel*. 2025;379:133092.https://doi.org/10.1016/j.fuel.2024.133092

Loo DL, Teoh YH, How HG, Le TD, Nguyen HT, Rashid T, Pottmaier D, Sher F. Effect of nanoparticles additives on tribological behaviour of advanced biofuels. *Fuel*. 2023;334:126798.https://doi.org/10.1016/j.fuel.2022.126798

Lyu X, Xu P, Wang Y, Bao W, Ge C, Ma X, Yong Q, Wang Y, You Q, Xie K. The anti-friction and anti-wear mechanism of lubricate oil additives in the piston ring–cylinder liner system of engines. *Ind LubrTribol*. 2026;78(4):509-530.https://doi.org/10.1108/ILT-12-2024-0496

Modi V, Rampure PB, Babbar A, Kumar R, Nagaral M, Bhowmik A, Pandey S, Hasnain SM, Ali MM, Bashir MN. Nanoparticle-enhanced biodiesel blends: a comprehensive review on improving engine performance and emissions. *Mater Sci Energy Technol*. 2024;7:257-273.https://doi.org/10.1016/j.mset.2024.02.001

Mulk WU, Ismael MA, Aziz ARA, Azman M, Aider M, Younas M, Hamdy M, Nemitallah MA. Recent progress in biodiesel-fueled ICEs and role of nano-additives in optimizing combustion and emissions with cost analysis: a comprehensive review. *Renewable Sustainable Energy Rev*. 2026;226:116263.https://doi.org/10.1016/j.rser.2025.116263

Paul A, Patil V, Singh P, Panua R, Kumar S. Thermodynamic and sustainability analysis of sanitary waste derived syngas-hydrogen blends with diesel in a RCCI engine. *International Journal of Hydrogen Energy*. 2026;198:152725.https://doi.org/10.1016/j.ijhydene.2025.152725

Pawar C, Shreeprakash B, Mokshanatha B, Nikam KC, Motgi N, Jathar LD, Shelare SD, Sharma S, Dwivedi SP, Bains PS, Kumar A. Machine learning-based assessment of the influence of nanoparticles on biodiesel engine performance and emissions: a critical review. *Archives of Computational Methods in Engineering*. 2025;32(1):499–533.https://doi.org/10.1007/s11831-024-10144-0

Peña-Parás L, Taha-Tijerina J, Garza L, Maldonado-Cortés D, Michalczewski R, Lapray C. Effect of CuO and Al_2O_3 nanoparticle additives on the tribological behavior of fully formulated oils. *Wear*. 2015;332:1256–1261.https://doi.org/10.1016/j.wear.2015.02.038

Polat F. Experimental evaluation of the impacts of diesel–nanoparticles–waste tire pyrolysis oil ternary blends on the combustion, performance, and emission characteristics of a diesel engine. *Process Safety and Environmental Protection*. 2022;160:847–858. https://doi.org/10.1016/J.PSEP.2022.02.002

Ravikiran, Prakash KR, Vaibhav KM, Sachin B, Prasad CD, Babu RN. Enhancing biodegradable lubricants with SiO_2 and TiO_2 nanoparticles: effects on viscosity, tribological behavior, rheological performance, and sustainability. *Biomass Conversion and Biorefinery*. 2025;15(24):31575–31590.https://doi.org/10.1007/s13399-025-06804-1

Sachuthananthan B, Krupakaran RL, Balaji G. Exploration on the behaviour pattern of a DI diesel engine using magnesium oxide nano additive with plastic pyrolysis oil as alternate fuel. *International Journal of Ambient Energy*. 2021;42(6):701–712.https://doi.org/10.1080/01430750.2018.1563812

Saha D, Sinha A, Roy B. Critical insights into the effects of plastic pyrolysis oil on emission and performance characteristics of CI engine. *Environmental Science and Pollution Research*. 2021;28(33):44598–44621.https://doi.org/10.1007/s11356-021-14919-x

Sambandam P, Punitha N, Vijetha K, Baskar S, Shamprasshaath SV, Seikh AH, Ifseisi AA, Sharma A. Effect of graphite nanoadditives on the behavior of a diesel engine fueled with pyrolysis fuel recovered from used plastics. *ACS Omega*. 2024;9(38):39584–39595.https://doi.org/10.1021/acsomega.4c03715

Sathish T, Ağbulut Ü, Giri J, Al-lehaibi M, Hourani AO, Hoang AT. Potential waste-to-wealth strategy for combining medical surgical gloves-derived pyrolysis oil with pentanol and nanoparticles: experimental analysis on engine behaviors. *Global Challenges*. 2025:e00031. https://doi.org/10.1002/gch2.202500031

Sikdar S, Menezes PL. "The role of functionalized CuO additive in enhancing tribological performance of plastic oil lubricant." *Lubrication Science*. 2025;37(2):170–188. https://doi.org/10.1002/ls.1732Digital Object Identifier (DOI)

Sikdar S, Rahman MH, Ralls AM, Menezes PL. "Enhancement in tribological performance of plastic oil by solid lubricant additives." *Lubrication Science*. 2023;35(7):420–437. https://doi.org/10.1002/ls.1647

Soundararajan G, Bibin C, Kumar RA, Arunkumar S, Rajesh K, Devarajan Y, Mishra R.

"Synergistic effects of graphene quantum dot additives in waste plastic oil blends: Combustion stability and emission reductions analysis." *Results in Engineering*. 2025;25:104130. https://doi.org/10.1016/j.rineng.2025.104130

Suhel A, Rahim NA, Rahman MRA, Ahmad KAB, Khan U, Teoh YH, Abidin NZ. "Impact of ZnO nanoparticles as additive on performance and emission characteristics of a diesel engine fueled with waste plastic oil." *Heliyon*. 2023;9(4):e14782. https://doi.org/10.1016/j.heliyon.2023.e14782

Sundar SP, Palanimuthu V, Sathyamurthy R, Hemalatha D, Kumar RS, Bharathwaaj R, Chamkha AJ. "Feasibility study of neat plastic oil with TiO_2 nanoadditive as an alternative fuel in internal combustion engine." *Journal of Thermal Analysis and Calorimetry*. 2022;147(3):2567–2578. https://doi.org/10.1007/s10973-021-10657-x

Thilipkumar P, Karuppusamy M. "Impact of graphene oxide nanoparticles on performance, combustion, emissions, and tribological characteristics of SAME20 algae biodiesel." *Environmental Science and Pollution Research*. 2026;33(13):6302–6326. https://doi.org/10.1007/s11356-026-37697-w

Thiruselvam K, Ganesan S, Vengadesan E, Senthil S. "Enhancement of compression ignition engine performance and emission reduction using pyrolyzed waste plastic oil blended with aluminum oxide nanoparticles." *Environmental Progress & Sustainable Energy*. 2025;44(4):e70008. https://doi.org/10.1002/ep.70008

Tarun John Thomas, Thangapandian N, Sakthivel D, Mohideen SMSF, Basha S, Brindhadevi K, Ramya G. "Experimental analysis of C.I. engine using pyrolyzed plastic oil blended with alumina nano additive." *Fuel*. 2022;312:122929. https://doi.org/10.1016/j.fuel.2021.122929

Verma A, Jiang W, Abu Safe HH, Brown WD, Malshe AP. "Tribological behavior of deagglomerated active inorganic nanoparticles for advanced lubrication." *Tribology Transactions*. 2008;51(5):673–678. https://doi.org/10.1080/10402000801947691

Wechselberger C, Lang T, Popadić S, Lipp AM. "Environmental impacts of plastic degradation: Toxic byproducts, environmental risks, and eco-friendly alternatives." *Microplastics*. 2026;5(1):40. https://doi.org/10.3390/microplastics5010040

Wierzbicki S, Duda K. "Renewable fuels for internal combustion engines: 2nd edition." *Energies*. 2026;19(2):330.https://doi.org/10.3390/en19020330

Yadav P, Kumar N, Gautam R. "Improvement in performance of CI engine using various techniques with alternative fuel." *Energy Sources, Part A: Recovery, Utilization, and Environmental Effects*. 2025;47(1):4129–4154. https://doi.org/10.1080/15567036.2020.1864517

Yaqoob H, Heng TY, Teobaldi G. "Friction and wear characteristics of tire pyrolysis oil." *Tribology International*. 2022;176:107930. https://doi.org/10.1016/j.triboint.2022.107864

Yilmaz AC. "Comprehensive analyses of characterization and conjoint influence of nanofuels and nanolubricants on acoustic, tribological behavior, performance and emission characteristics of a compression ignition engine." *Fuel*. 2025;381:133665. https://doi.org/10.1016/j.fuel.2024.133665

Yim H, Valizadeh S, Cho K, Park YK. "Production of low-aromatic oil from catalytic pyrolysis of waste plastics-derived wax." *Journal of Analytical and Applied Pyrolysis*. 2025;186:106964.https://doi.org/10.1016/j.jaap.2025.106964

Zafar M, Hussain A, Ahmed T, Daabo A, Ullah F. "Addition of nanoparticles to biodiesel–diesel blends to improve engine efficiency and reduce tailpipe emission." In: *Machine Learning for Sustainable Energy Solutions*. 2026. p. 139–159. https://doi.org/10.1002/9781394267439.ch8

Acknowledgements

The authors have no acknowledgements to declare.

Funding

Not applicable

Authors' Contributions

Thirugnanasambantham Rajamanickam**:** Developing the concept, Methodology, Experimental analysis, and drafting the manuscript. Santhoshkumar Annamalai**:** Evaluation, Data analysis, Validation, and Manuscript editing. Jayakumar Thangamani**:** Supervision, Monitoring,

and Critical revision of the manuscript. Arunprasad Jayaraman**:** Interpretation of results, Technical support, and Final manuscript editing.

Ethical Approval

Not applicable.

Consent to Participate

Not applicable.

Consent to Publish

Not applicable.

Competing Interests

The authors declare no known competing financial interests or personal relationships that could have influenced the work reported in this paper.

Data Availability Statement

Upon reasonable request, the authors will provide all relevant data.